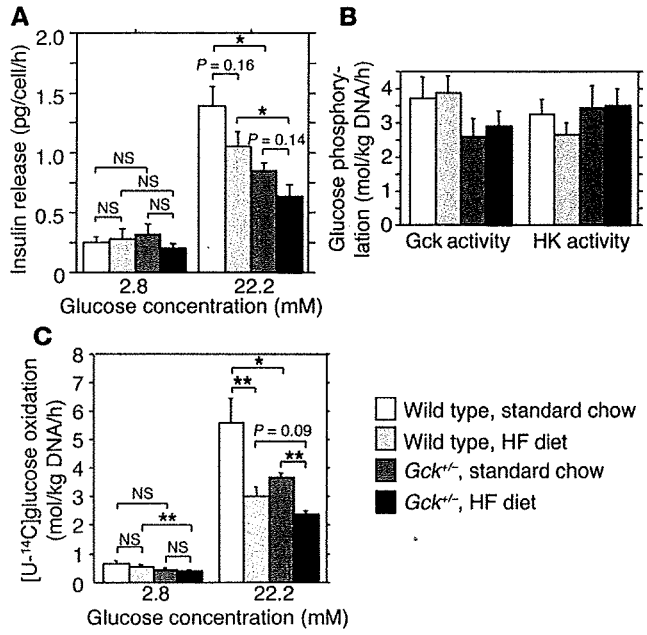

Figure 3

Decreased insulin secretion and glucose oxidation in *Gck*$^{+/-}$ islets. (**A**) Static incubation study of islets from wild-type and *Gck*$^{+/-}$ mice after 4 weeks on standard chow or HF diet. Static incubation of 10 islets/tube was performed at 37°C for 1 hour with various glucose concentrations after preincubation with a 2.8-mM glucose concentration for 20 minutes. Results are shown as pg insulin/cell/h (n = 4). (**B**) Gck and hexokinase (HK) activity of islets. Glucose phosphorylation activity was assessed in pancreatic islets from wild-type and *Gck*$^{+/-}$ mice after 20 weeks on standard chow or HF diet. Results are shown as mol/kg DNA/h (n = 16–20). (**C**) Glucose oxidation by pancreatic islets from wild-type and *Gck*$^{+/-}$ mice after 20 weeks on standard chow or HF diet. Results are shown as mol/kg DNA/h (n = 10). *P < 0.05; **P < 0.01.

β cell mass compared with wild-type mice on standard chow, whereas even after 40 weeks the *Gck*$^{+/-}$ mice showed only a 2-fold increase in β cell mass (Figure 2C). The number of cells per islet was significantly increased in wild-type mice on the HF diet compared with those on standard chow, but the difference between the 2 *Gck*$^{+/-}$ groups was not significant (Figure 2D). DNA content per islet was also significantly higher in wild-type mice than in *Gck*$^{+/-}$ mice on the HF diet (HF diet–fed wild-type, 39.1 ± 2.3 ng/islet, n = 6; HF diet–fed *Gck*$^{+/-}$, 22.7 ± 1.9 ng/islet, n = 6; P < 0.001). To estimate the contribution of the size of individual β cells to the increase in β cell mass, we divided the β cell area by the number of β cell nuclei it contained. However, since the results showed little difference in β cell size between wild-type and *Gck*$^{+/-}$ mice on the HF diet (HF diet–fed wild-type, 155 ± 4 μm^2, n = 101; HF diet–fed *Gck*$^{+/-}$, 149 ± 4 μm^2, n = 105; P = NS), the increased β cell mass in wild-type mice on the HF diet was attributed to an increase in the number of cells (hyperplasia) rather than to an increase in the volume of individual cells (hypertrophy).

The number of β cells present is governed by a balance among β cell replication (increase in number of β cells by preexisting β cells), neogenesis (generation of β cells by non–β cells, such as acinar cells and duct cells), and apoptosis. We estimated β cell proliferation on the basis of BrdU incorporation and proliferating cell nuclear antigen (PCNA) staining. On the HF diet, there were significantly more insulin and BrdU double-positive cells in the wild-type mice than in the *Gck*$^{+/-}$ mice (Figure 2E), and similar results were obtained by PCNA staining (Figure 2F). Single-strand DNA analysis revealed no difference in the percentage of apoptotic cells in islets between wild-type and *Gck*$^{+/-}$ mice on the HF diet (HF diet–fed wild-type, 0.031% ± 0.026%, n = 86; HF diet–fed *Gck*$^{+/-}$, 0.018% ± 0.018%, n = 33; P = NS). Fewer than 1 in 3,000 cells in the islets of both mouse groups were found to be apoptotic with an in situ cell death detection kit. Thus, in contrast to the wild-type mice, the failure of compensatory β cell hyperplasia in the *Gck*$^{+/-}$ mice on the HF diet was associated with a lack of compensatory increase in β cell proliferation.

Impaired glucose-stimulated insulin secretion associated with decreased glucose metabolism in the β cells of Gck$^{+/-}$ *mice on the HF diet.* Next, we investigated glucose-stimulated insulin secretion (GSIS) by individual β cells. After 4 weeks, GSIS at 22.2 mM glucose normalized by cell number was lower in wild-type mice on the HF diet than in those fed standard chow (Figure 3A). Thus, the hyperinsulinemia in the wild-type mice on the HF diet can be explained by increased β cell mass, not by increased insulin secretion by individual β cells. GSIS at 22.2 mM glucose normalized by cell number was significantly lower in *Gck*$^{+/-}$ mice than in wild-type mice on both diets, a finding consistent with the results of our previous study (24). The hyperglycemia itself may have also affected the insulin secretory function of islets in the *Gck*$^{+/-}$ groups. GSIS at 22.2 mM glucose was lower in the islets of the HF diet groups than in those of the standard chow groups of both genotypes, and after 20 weeks it was significantly decreased in the HF diet groups compared with the standard chow groups (data not shown), a finding consistent with previous reports that prolonged exposure to FFA results in suppression of insulin release (25, 26). While islet hexokinase activity was similar in all 4 groups, Gck activity in the *Gck*$^{+/-}$ standard chow and HF diet groups was 30% and 25% lower than in the wild-type standard chow and HF diet groups, respectively, although the differences were not statistically significant (Figure 3B). When islets of essentially the same size were prepared and [U-^{14}C]glucose oxidation was assayed in their mitochondria, glucose oxidation at 22.2 mM glucose was significantly lower in the HF diet than in standard chow groups of both phenotypes (Figure 3C). Importantly, after 20 weeks on the HF diet, glucose oxidation at 22.2 mM glucose did not significantly differ between wild-type and *Gck*$^{+/-}$ mice (Figure 3C), suggesting that normal glucose oxidation levels are not necessary for the compensatory increase in β cell mass, although they may be essential for GSIS.

Gene expression profiles of the islets of HF diet–fed mice. We performed a DNA microarray analysis as a means of systematically examining the gene expression profiles of the islets. Of the 12,490 genes examined, 81 were overexpressed (by 3-fold or more; Supplemental Table 1; supplemental material available online with this article; doi:10.1172/JCI17645DS1) and 63 were underexpressed (by 3-fold or more; Supplemental Table 2) in the islets of *Gck*$^{+/-}$ mice on the HF diet compared with the islets of wild-type mice on the HF diet. Interestingly, markedly lower expression of *Irs2* (25-fold decrease, the greatest decrease in expression level of the genes examined), *Pdpk1* (3-fold decrease), and *Hgf* (3.1-fold decrease) was observed in *Gck*$^{+/-}$ islets compared with those of wild-type mice, yet there were no differences in expression of *Insr*, *Irs1*, *Irs3*, *Pik3r1*, *Pik3r2*, *Pik3ca*, or *Akt1* (Table 1). Expression of *Igf1r* (2.4-fold decrease) and *Prlr* (2.6-fold decrease) was also modestly lower in *Gck*$^{+/-}$ islets than in wild-type islets. By contrast, there was no difference between the 2 HF diet–fed groups in expression of apoptosis-related genes

Table 1
Changes in gene expression levels in islets based on DNA microarray analysis

Gene	Ratio
Insulin signaling	
Irs2	–25
Pdpk1	–3
Igf1r	–2.4
Insr, Insrr, Irs1, Irs3, Pik3r1, Pik3r2, Pik3ca, Akt1, Foxo1, Prkca, Prkcb1, Prkcc, Prkcd, Prkce, Prkci, Prkcq, Prkcz, Rps6ka1, Map2k3, Map2k6, Mapk10	NC
Non–insulin signaling	
Hgf	–3.1
Prlr	–2.6
Ghr, Btc, Stat5b, Fgf8, Fgf10	NC
Transcription factors	
Ipf1, FoxO1, Hnf1b, Hnf3a, Hnf3b, Neurog3, Pax4, Pax6, Nkx2-2, Nkx6-1, Hes1, Hes2, Cebpa, Cebpb, Cebpd	NC
Apoptosis-related genes	
Bad, Casp3, Casp6	NC
Cell cycle–related genes	
Ccnd2	–5.8
Ccnd1, Ccnd3, Cdk4, Cdkn1a, Cdkn1b, Cdkn2a, Cdkn2b, Cdkn2d	NC
cAMP-related genes	
Glp1r, Prkar1a, Prkar1b, Prkar2a, Prkaca, Prkacb, Lasp1, Creb1, Crebbp	NC
Membrane proteins	
Slc2a2	NC
Translation initiation factors	
Eif1a, Eif4a1, Eif4a2	NC

Ratios are based on comparisons of $Gck^{+/-}$ mice versus wild-type mice after 20 weeks on the HF diet. NC, no significant change.

such as *Casp3* and *Bad* in the islets. RT-PCR analysis confirmed the upregulation of Irs2, Igf1r, and Prlr expression in the islets of wild-type mice on the HF diet compared with those on standard chow as well as reduced expression in the islets of $Gck^{+/-}$ mice on the HF diet compared with those of HF diet–fed wild-type mice (Figure 4A). Quantitative PCR analysis, which amplified another region of the *Irs2* and *Igf1r* genes, revealed that expression of *Irs2* and *Igf1r* in the islets of $Gck^{+/-}$ mice on the HF diet was 60.6% ($P < 0.01$ versus wild-type mice) and 76.4%, respectively, that of their expression level in the islets of wild-type mice on the HF diet.

Next, we examined the protein levels by Western blotting. We prepared islets (less than 250 μm in diameter) from mice after 20 weeks on each diet. The results confirmed upregulation of Irs2 and Igf1r expression in the islets of wild-type mice on the HF diet compared with those on standard chow as well as reduced expression in the islets of $Gck^{+/-}$ mice on the HF diet compared with those of wild-type mice on the HF diet (Figure 4, B and C). Interestingly, expression of *Insr* was significantly increased in the HF diet–fed groups compared with standard chow–fed groups (Figure 4, B and C), although there were no differences in expression of *Akt1* among the 4 groups. *Ipf1* expression was indistinguishable between the islets of $Gck^{+/-}$ and wild-type mice on standard chow, but the protein level was slightly, but significantly, lower in the islets of $Gck^{+/-}$ mice on the HF diet than in those of wild-type mice on the HF diet (Figure 4, B and C). Immunostaining revealed clearly lower *Ipf1* nuclear expression in the β cells of $Gck^{+/-}$ mice on the HF diet than in those of wild-type mice on the HF diet (Supplemental Figure 1).

In summary, DNA microarray and RNA and protein analyses revealed upregulation of *Irs2* and *Igf1r* expression in the islets of wild-type mice on the HF diet compared with those fed standard chow as well as reduced expression in the islets of $Gck^{+/-}$ mice on the HF diet compared with those of HF diet–fed wild-type mice.

Insufficient increase in β cell mass in $Irs2^{+/-}$ mice on the HF diet. Next we investigated the role of Irs2 in the regulation of β cell mass in mice on the HF diet. After 10 weeks on the HF diet, $Irs2^{+/-}$ mice exhibited increases in body weight, blood glucose, serum insulin, and insulin resistance similar to those of HF diet–fed wild-type mice (Figure 5, A–D). The $Irs2^{+/-}$ mice had β cell area and maximum islet diameter similar to those of wild-type mice fed standard chow, but the increases were significantly smaller than those observed in HF diet–fed wild-type mice (Figure 5, E and F). After only 5 weeks on the HF diet, $Irs2^{-/-}$ mice showed marked aggravation of glucose intolerance (27). While the mean of the maximum islet diameter was 14% greater in wild-type mice on the HF diet than in those on standard chow, a difference that was significant, there was no such increase in the $Irs2^{-/-}$ mice on the HF diet compared with those on standard chow (data not shown). These results support a role for Irs2 in the increase in β cell mass on the HF diet.

Transgenic rescue by crossing $Gck^{+/-}$ mice with β cell Irs2 transgenic mice. To directly test our hypothesis that reduction of *Irs2* explains the impaired β cell hyperplasia in $Gck^{+/-}$ mice on HF diet, we crossed $Gck^{+/-}$ mice with β cell Irs2 transgenic (βIrs2Tg) mice, which express Irs2 in β cells under the control of the rat insulin promoter, and generated 2 lines of βIrs2Tg mice (Supplemental Figure 2, A and B). While the β cells of βIrs2Tg6 mice expressed a low level of Irs2 (2.2-fold upregulation compared with wild-type littermates), the β cells of βIrs2Tg12 mice expressed a high level of Irs2 (>17-fold upregulation). We chose to use the βIrs2Tg6 line because the 2.2-fold upregulation of Irs2 in βIrs2Tg6 mice was comparable to the *Irs2* expression level in wild-type mice on the HF diet. We crossed βIrs2Tg6 mice with $Gck^{+/-}$ mice and obtained 4 genotypes: wild-type, βIrs2Tg, $Gck^{+/-}$, and βIrs2Tg$Gck^{+/-}$. Only male mice were used in the experiments. After 20 weeks on the HF diet, the fold change in Irs2 protein expression compared with $Gck^{+/-}$ mice was 3.5 ± 0.2 for wild-type, 4.6 ± 0.5 for βIrs2Tg, 1.0 ± 0.1 for $Gck^{+/-}$, and 3.1 ± 0.6 for βIrs2Tg$Gck^{+/-}$ mice (Supplemental Figure 2, C and D). These results can be explained by the fact that HF diet upregulated endogenous Irs2 expression in the islets of wild-type and βIrs2Tg mice, but not the islets of $Gck^{+/-}$ or βIrs2Tg$Gck^{+/-}$ mice. After 4 weeks on the HF diet, the glucose tolerance of βIrs2Tg mice was similar to that of wild-type mice, but the βIrs2Tg$Gck^{+/-}$ mice had better glucose tolerance than did $Gck^{+/-}$ mice (data not shown). After 20 weeks on the HF diet, the βIrs2Tg mice had glucose tolerance similar to that of wild-type mice, but the βIrs2Tg$Gck^{+/-}$ mice had better glucose tolerance and higher serum insulin levels than did $Gck^{+/-}$ mice (Figure 6, A and B). Thus, overexpression of Irs2 partially prevented diabetes in $Gck^{+/-}$ mice on the HF diet.

Figure 6C shows representative insulin staining of the pancreas after 20 weeks on the HF diet. Measurement of the β cell area showed that it was significantly increased in βIrs2Tg$Gck^{+/-}$ mice compared with $Gck^{+/-}$ mice (Figure 6D), and consistent with this finding, there were significantly more insulin and BrdU double-positive cells in

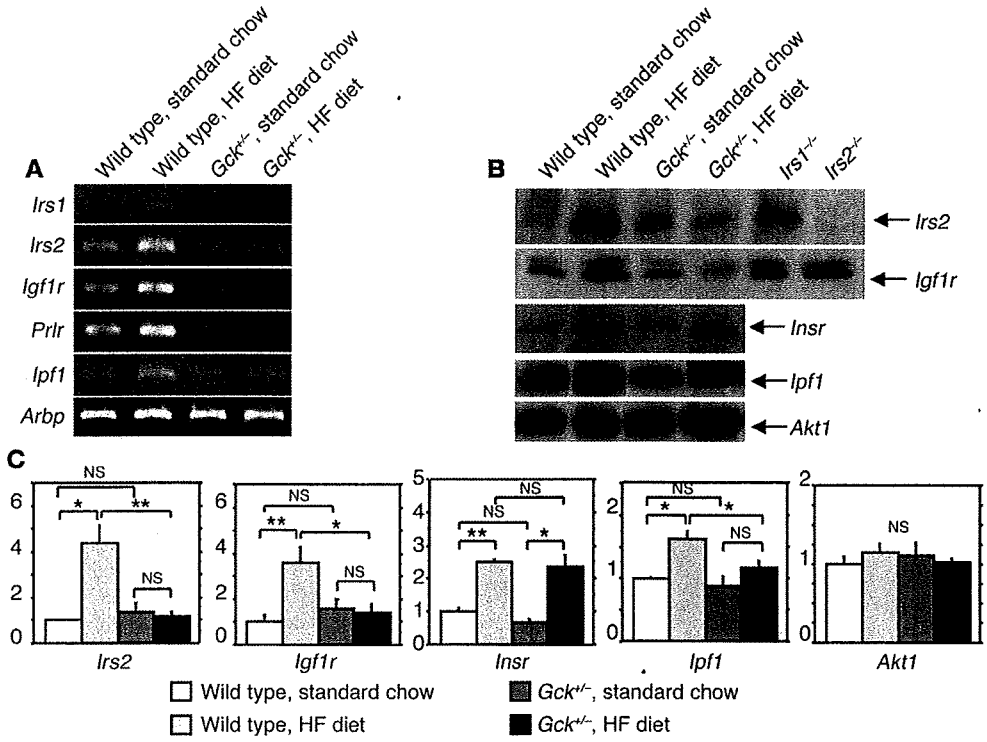

Figure 4

Changes in gene expression levels in the islets of *Gck*$^{+/-}$ mice on the HF diet. (**A**) RT-PCR analysis of *Irs1*, *Irs2*, *Igf1r*, *Prlr*, *Ipf1*, and *Arbp* (36B4), shown as a control. Islets were isolated from wild-type or *Gck*$^{+/-}$ mice after 20 weeks on standard chow or HF diet. Experiments were replicated at least 3 times, and typical images are shown. (**B**) Western blot analysis of *Irs2*, *Igf1r*, *Insr*, *Ipf1*, and *Akt1*. Islets were isolated from wild-type or *Gck*$^{+/-}$ mice after 20 weeks on standard chow or HF diet, *Irs1*$^{-/-}$ mice, and *Irs2*$^{-/-}$ mice on standard chow (n = 3). Equal amounts of lysates (20 μg) were blotted with the antibody indicated. Quantitative determination of the β cell mass of islets less than 250 μm in diameter revealed the values in the 4 mouse groups to be indistinguishable (standard chow–fed wild-type, 0.81% ± 0.03%; HF diet–fed wild-type, 0.85% ± 0.03%; standard chow–fed *Gck*$^{+/-}$, 0.82% ± 0.02%; HF diet–fed *Gck*$^{+/-}$, 0.84% ± 0.02%). (**C**) Each expression level was quantified (n = 4–6). $^{*}P < 0.05$; $^{**}P < 0.01$.

βIrs2Tg*Gck*$^{+/-}$ mice than in *Gck*$^{+/-}$ mice (Figure 6, C and E). Next we isolated islets from the 4 mouse groups after 20 weeks on the HF diet and carried out static incubation experiments. GSIS at 11.1 mM glucose was not restored in βIrs2Tg*Gck*$^{+/-}$ mice compared with *Gck*$^{+/-}$ mice (Figure 6F), indicating that overexpression of Irs2 failed to restore β cell function in *Gck*$^{+/-}$ mice.

Mechanisms of Irs2 upregulation in the β cells of HF diet–fed mice. We examined known regulators of Irs2 expression, such as cAMP, and subsequent phosphorylation of cAMP response element–binding protein (CREB) (28) and FoxO1 (29). Although the cAMP content of the islets was unaffected by the HF diet (data not shown) and the levels of expression of cAMP-responsive genes — including *Creb1*, *Glp1r*, *Prkar1a*, *Prkar1b*, *Prkar2a*, *Prkaca*, *Prkacb*, and *Lasp1* — were unaltered (Table 1), Ser133 phosphorylation of CREB was impaired in *Gck*$^{+/-}$ mice compared with wild-type mice (Figure 7, A and B). FoxO1 is an activator of Irs2 in liver, because the Irs2 promoter is activated by FoxO1 through an insulin response element (29), but it has also been characterized as a key distal mediator of insulin signaling, because FoxO1 haploinsufficiency reverses β cell failure in *Irs2*$^{+/-}$ mice (30). Immunohistochemical analysis revealed that FoxO1 was more localized in the nuclei of β cells of *Gck*$^{+/-}$ mice on the HF diet than in those of wild-type mice on the HF diet (Figure 8A). In fact, the ratio of nuclear FoxO1-positive cells to the total number of islet cells was significantly higher in *Gck*$^{+/-}$ mice on the HF diet than in wild-type mice on the HF diet (Figure 8B). Overexpression of Irs2 in β cells decreased the number of nuclear FoxO1-positive cells in the *Gck*$^{+/-}$ mice on the HF diet, indicating that upregulation of Irs2 in β cells stimulated FoxO1 nuclear exclusion (Figure 8, A and B).

The above findings, together with the fact that cAMP and calcium pathways trigger CREB Ser133 phosphorylation, thereby upregulating Irs2 (28), suggest that impaired CREB Ser133 phosphorylation is a plausible explanation for the insufficient upregulation of Irs2 in *Gck*$^{+/-}$ mice on the HF diet. The significance of the decreased FoxO1 nuclear exclusion in *Gck*$^{+/-}$ mice on the HF diet are discussed below.

Discussion

Gck is known to function as a glucose sensor in insulin secretion by pancreatic β cells (4), but to our knowledge, its involvement in the regulation of β cell mass had previously not been recognized. In this paper, we report 4 findings, which we believe to be novel, that link Gck to β cell mass. First, we found that wild-type mice on a HF diet showed marked compensatory β cell hyperplasia associated with increased replication of β cells, whereas *Gck*$^{+/-}$ mice failed to show as much β cell hyperplasia despite showing a similar degree of insulin resistance (Figure 2). The finding that haploinsufficiency of Gck led to insufficient β cell hyperplasia on the HF diet suggests a critical requirement for Gck, not only for GSIS, but for β cell hyperplasia in response to HF diet–induced insulin resistance to protect against diabetes. Although glucose itself has been recognized to be a nutrient for β cells, to our knowledge it was previously unknown whether glucose metabolism is crucial for β cell growth (7). The results of this study in regard to the role of glucose metabolism and Gck in the regulation of β cell mass clearly demonstrate that Gck is associated with β cell mass and proliferation, raising the possibility that other enzymes involved in glucose metabolism may have a similar effect on β cell growth. Second, we found that on the HF diet, expression of *Irs2* and *Igf1r* was upregulated in wild-type islets but markedly lower in the islets of *Gck*$^{+/-}$ mice (Table 1 and Figure 4, A–C), showing that Gck is required for the coordinated upregulation of Irs2 and Igf1r in the islets of HF diet–fed mice. Secondary effects of chronic hyper-

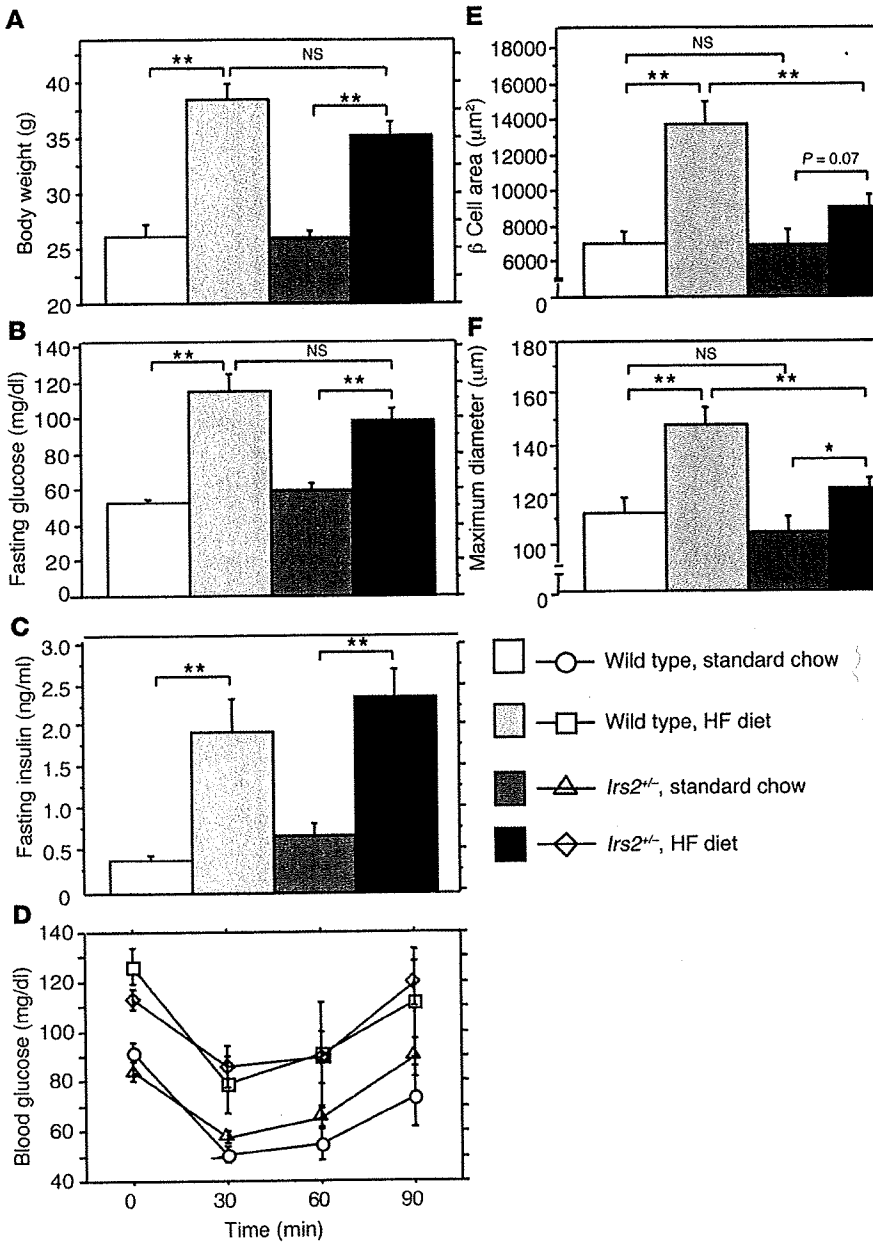

Figure 5
Insufficient β cell hyperplasia in *Irs2*$^{+/-}$ mice on the HF diet. (**A–C**) Body weight (**A**), fasting blood glucose (**B**), and serum insulin (**C**) values of wild-type and *Irs2*$^{+/-}$ mice after 10 weeks on standard chow or HF diet (n = 5–8). (**D**) Insulin tolerance in wild-type and *Irs2*$^{+/-}$ mice after 10 weeks on standard chow or HF diet (n = 4–8). (**E** and **F**) Area of β cells in each islet (**E**) and maximum islet diameter (**F**) in wild-type and *Irs2*$^{+/-}$ mice after 10 weeks on standard chow or HF diet. We examined 100–150 islets from 3 animals per group. Values represent mean ± SEM. $^{*}P < 0.05$; $^{**}P < 0.01$.

glycemia may also have contributed to the decreased *Irs2* and *Igf1r* expression in the islets of *Gck*$^{+/-}$ mice on the HF diet. It should be noted, however, that wild-type mice after 20 weeks on the HF diet and *Gck*$^{+/-}$ mice on standard chow had similar glucose tolerance (Figure 1F) and that after another 20 weeks the HF diet–fed wild-type mice showed a greater increase in β cell mass, whereas even after 40 weeks on the HF diet the *Gck*$^{+/-}$ mice showed only a small increase (Figure 2C). These results indicate that chronic hyperglycemia alone cannot fully explain the insufficient β cell hyperplasia of *Gck*$^{+/-}$ mice on the HF diet. Third, in a previous study we showed a lack of β cell hyperplasia in response to genetically determined insulin resistance in *Irs2*$^{-/-}$ mice (11), and in the present study we demonstrated that haploinsufficiency of Irs2 led to insufficient β cell hyperplasia on the HF diet (Figure 5, E and F). Fourth, we found that overexpression of Irs2 partially prevented diabetes in *Gck*$^{+/-}$ mice on the HF diet. It should be noted, however, that the slight improvement in glucose tolerance can be explained by the fact that β cell mass, not β cell function, was restored in βIrs2Tg*Gck*$^{+/-}$ mice compared with *Gck*$^{+/-}$ mice on the HF diet (Figure 6, C–E). These results provide genetic evidence that Irs2 is critically involved in β cell hyperplasia on the HF diet. Based on these findings, we propose that both Gck and Irs2 are critical requirements for β cell hyperplasia in response to HF diet–induced insulin resistance.

What is the mechanism of Irs2 upregulation on the HF diet? We previously reported that the increase in intracellular calcium concentration in response to glucose was impaired in islets of *Gck*$^{+/-}$ mice (ref. 3 and our unpublished observations). In the present study we noted the impaired CREB Ser133 phosphorylation in *Gck*$^{+/-}$ mice on the HF diet. Taken together with the fact that cAMP and calcium pathways trigger CREB Ser133 phosphorylation, thereby upregulating Irs2

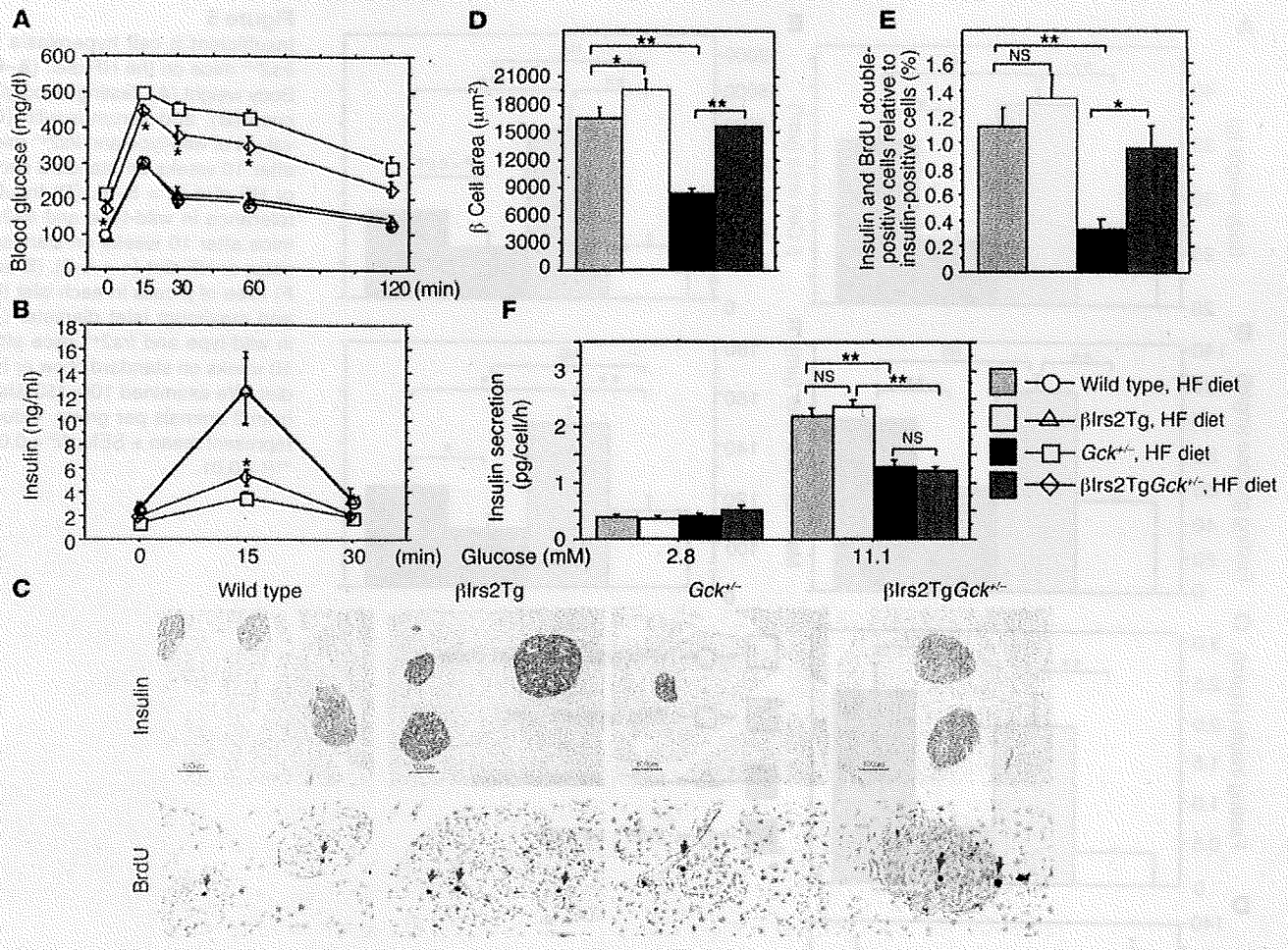

Figure 6

Transgenic rescue by crossing *Gck*$^{+/-}$ mice with βIrs2Tg mice. (**A** and **B**) Glucose tolerance in wild-type, *Gck*$^{+/-}$, βIrs2Tg, and βIrs2Tg*Gck*$^{+/-}$ mice after 20 weeks on HF diet. (**A**) Plasma glucose levels. (**B**) Serum insulin levels. $n = 31$ (wild-type), 20 (βIrs2Tg), 35 (*Gck*$^{+/-}$), 16 (βIrs2Tg*Gck*$^{+/-}$). $^*P < 0.05$, *Gck*$^{+/-}$ versus βIrs2Tg*Gck*$^{+/-}$. (**C**) Histologic analysis of wild-type, *Gck*$^{+/-}$, βIrs2Tg, and βIrs2Tg*Gck*$^{+/-}$ mouse islets after 20 weeks on HF diet. Representative pancreatic islets are shown. Top panels show insulin staining; bottom panels show BrdU staining. Scale bars: 100 μm. Original magnification, ×100 (top panels); ×400 (bottom panels). (**D**) Area of β cells in each islet after 20 weeks on HF diet. We examined 100–150 islets from 3 animals per group. (**E**) Replication rate of β cells, assayed on the basis of BrdU incorporation after 20 weeks on HF diet. Results are shown as ratios of insulin and BrdU double-positive cells to insulin-positive cells ($n = 4$). (**F**) Static incubation study of islets after 20 weeks on the HF diet. Static incubation of 10 islets/tube was performed at 37°C for 1 hour with various glucose concentrations after preincubation with a 2.8-mM glucose concentration for 20 minutes. Results are shown as pg insulin/cell/h ($n = 4$). Values represent mean ± SEM. $^*P < 0.05$; $^{**}P < 0.01$.

(28), our present results suggest that the impaired calcium signaling caused by haploinsufficiency of Gck in combination with HF diet–induced insulin resistance leads to the impaired Ser133 phosphorylation of CREB. Further study is needed to test this hypothesis.

What, then, is the molecular link between Irs2 and β cell proliferation? We noted the decreased FoxO1 nuclear exclusion in *Gck*$^{+/-}$ mice on the HF diet compared with wild-type mice on the HF diet (Figure 8, A and B). This finding, together with previous reports of a role of FoxO1 downstream of Irs2 in linking insulin signaling to Ipf1 regulation of β cells and compensation to insulin resistance (30, 31), suggests that decreased FoxO1 nuclear exclusion contributes to the insufficient proliferative response of existing β cells to insulin resistance in *Gck*$^{+/-}$ mice on the HF diet, and the fact that overexpression of Irs2 in β cells stimulated FoxO1 nuclear exclusion in wild-type and *Gck*$^{+/-}$ mice (Figure 8, A and B) is consistent with this hypothesis. Moreover, we noted lower Ipf1 nuclear expression in the β cells of *Gck*$^{+/-}$ mice on the HF diet than in those of wild-type mice on the HF diet (Supplemental Figure 1), which can be explained by the decreased FoxO1 nuclear exclusion in *Gck*$^{+/-}$ mice on the HF diet, as previously demonstrated in *Irs2*$^{-/-}$ mice (30). However, because haploinsufficiency of Ipf1 led to impaired β cell function, but not to decreased β cell mass (32), whether decreased Ipf1 nuclear expression is involved in the decreased β cell hyperplasia in *Gck*$^{+/-}$ mice on the HF diet remains unresolved. To determine whether Ipf1 is involved in the regulation of β cell mass in *Gck*$^{+/-}$ mice, we are now investigating the phenotypes obtained by crossing *Gck*$^{+/-}$ mice with β cell–specific Ipf1 transgenic mice.

Recently, β cell–specific ablation of Pdpk1 has been shown to induce diabetes as a result of loss of β cell mass (33); in the present study, expression of *Pdpk1* actually decreased in HF diet–fed *Gck*$^{+/-}$ mice compared with wild-type mice (Table 1). Thus, inadequate acti-

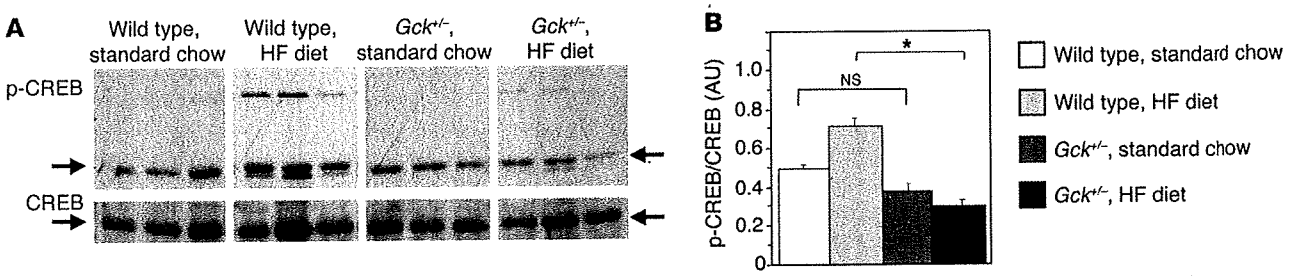

Figure 7
Impaired Ser133 phosphorylation of CREB in *Gck*$^{+/-}$ mice on HF diet. (**A**) Western blot assay of Ser133-phosphorylated CREB (p-CREB) and total CREB levels in islets from wild-type and *Gck*$^{+/-}$ mice after 20 weeks on standard chow or HF diet. (**B**) Quantitation of Ser133 phosphorylation of CREB in wild-type and *Gck*$^{+/-}$ mice after 20 weeks on standard chow or HF diet. Results are shown as proportions of the intensity of the Ser133-phosphorylated CREB band to that of the total CREB band ($n = 5$). Ser133 phosphorylation of CREB was significantly impaired in *Gck*$^{+/-}$ mice compared with wild-type mice on the HF diet. Values represent mean ± SEM. $^{*}P < 0.05$.

vation of Pdpk1 downstream of Irs2 signaling may also play a role in the insufficient compensatory β cell hyperplasia in *Gck*$^{+/-}$ mice on the HF diet. Interestingly, while expression of cyclin D1, cyclin D3, CDK4, and cyclin-dependent kinase inhibitors including p21 and p27 Kip1 was unaltered in the islets of *Gck*$^{+/-}$ mice on the HF diet compared with those of wild-type mice on the HF diet, expression of cyclin D2 was downregulated (5.8-fold decrease) and expression of p15 inhibitor was slightly upregulated (1.2-fold increase). The roles of these cell cycle–related molecules in β cell proliferation downstream of Irs2 signaling should be examined in a future study.

What is the relationship between glucose metabolism and β cell proliferation? It has been established that β cell function, including GSIS, can be explained by glucose metabolism (4). Glucose oxidation was decreased to a similar degree in both wild-type and *Gck*$^{+/-}$ mice on the HF diet (Figure 3C). Although the wild-type mice showed marked compensatory β cell hyperplasia, the *Gck*$^{+/-}$ mice failed to show such β cell hyperplasia, demonstrating that glucose oxidation is not directly linked to β cell mass. Moreover, Gck activity in the wild-type mice was not increased on the HF diet compared with standard chow (Figure 3B). From a biochemical standpoint, "classical" glucose metabolism cannot explain β cell proliferation on the HF diet, and some additional mechanism is required. It may be premature, however, to rule out an involvement of glucose metabolism in HF diet–induced β cell hyperplasia based on the studies of glucose oxidation in isolated islets, because there are no doubt important glucose signals left to be discovered, as evidenced from the pursuit of the mechanisms of KATP-independent GSIS. Although β cell function and β cell growth have previously been thought to be regulated differently, the results of the present study indicate that both may be regulated in part by a coordinated or common mechanism.

What is the relevance of our results to clinical practice in human diabetes? Relatively common mutations of the *Gck* gene have been reported in MODY patients (2, 34), but since they are not restricted to the β cell–specific isoform, the diabetic phenotype of these patients is due to a combination of defects in insulin secretion and glucose uptake by the liver. By contrast, a SNP in the promoter region of the *Gck* gene has been reported to be associated with reduced β cell function in Japanese-American men (35). The results of our study are somewhat surprising, as the majority of the known clinical cases of MODY have been mild cases of diabetes (2, 34). However, the severity of diabetes is also known to differ among patients with the same mutation, and the differences may be attributable to peripheral insulin resistance associated with obesity and/or environmental factors (34, 36). Because a HF diet is one of the

Figure 8
Nuclear FoxO1-positive cells increased in *Gck*$^{+/-}$ mice on the HF diet compared with wild-type mice on the HF diet, and overexpression of Irs2 in β cells decreased nuclear FoxO1-positive cells in *Gck*$^{+/-}$ mice on the HF diet. (**A**) Immunohistochemical analysis of FoxO1 in islets from wild-type mice, βIrs2Tg mice, *Gck*$^{+/-}$ mice, and βIrs2Tg*Gck*$^{+/-}$ mice after 20 weeks on the HF diet. Representative islets are shown. FoxO1-positive cells are stained brown. Original magnification, ×600. (**B**) Ratio of the number of nuclear FoxO1-positive cells to the total number of islet cells. $n = 43$ (wild-type, *Gck*$^{+/-}$), 23 (βIrs2Tg), 48 (βIrs2Tg*Gck*$^{+/-}$). Values represent mean ± SEM. $^{**}P < 0.01$.

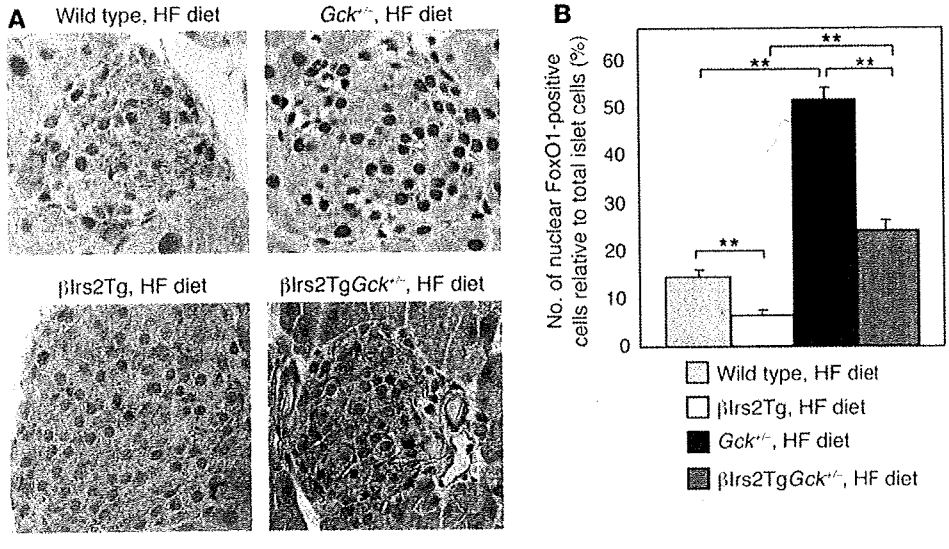

pivotal factors in the etiology of insulin resistance and obesity, our results should be relevant to the diversity in diabetes severity among MODY patients. Furthermore, since type 2 diabetes patients with decreased insulin secretion have been shown to have reduced β cell mass (37), $Gck^{+/-}$ mice on a HF diet should serve as a good animal model to better understand the relationship between decreased insulin secretion and decreased β cell mass in type 2 diabetes. Gck activation via small-molecule Gck activators in combination with increased cAMP production via glucagon-like peptide 1 derivatives may be a powerful strategy for the treatment of the decreased insulin secretion and decreased β cell mass in type 2 diabetes. In conclusion, the results of our study support the concept that Gck regulates β cell mass as well as β cell function. Irs2 was found to be involved in Gck-mediated β cell hyperplasia in HF diet–fed mice. Identification of the mechanism linking Gck and Irs2 should lead to novel therapeutic strategies that will increase β cell mass to compensate for HF diet–induced insulin resistance and may increase the amount of islets (β cells) for islet transplantation.

Methods

Animals. $Gck^{+/-}$ mice (129/Sv, ICR, and C57BL/6J hybrid background) were generated as described previously (3). Because of the heterogeneous genetic background of the mice, male offspring derived from $Gck^{+/-}$ intercrosses were analyzed in this study. The $Gck^{+/-}$ and wild-type mice were fed standard chow until 8 weeks of age and were then given free access to either standard chow or a HF diet. The animal care and procedures of the experiments were approved by the Animal Care Committee of the University of Tokyo. Animals were maintained by means of standard animal care procedures based on the institutional guidelines. $Irs1^{-/-}$ and $Irs2^{-/-}$ mice (CBA and C57BL/6J hybrid background) were generated as described previously (8, 11). The βIrs2Tg mouse lineage was established by fusing the 0.74-kb rat insulin II promoter to a mouse Irs2 cDNA (4 kb), microinjecting the purified *NotI* fragment into the pronucleus of eggs of fertilized C57BL/6J mice (CLEA Japan Inc.), and then crossing F1 offspring with C57BL/6J mice (Supplemental Figure 2, A and B). Male offspring littermates derived from crosses between male $Gck^{+/-}$ mice and female βIrs2Tg mice were analyzed in the Irs2 rescue experiments (Supplemental Figure 2, C and D).

Measurement of serum and islet parameters. Glucose, insulin, triglyceride, and FFA levels were determined with a Glutest Pro kit (SANWA KAGAKU KENKYUSHO CO. LTD), an insulin kit (Biotrak; Amersham Biosciences), and L-type TG M and NEFA C-test kits (Wako), respectively.

Diet protocol. The composition of the standard chow (CLEA Rodent Diet CE-2; CLEA Japan Inc.) was 50.7% (wt/wt) carbohydrate, 4.6% fat, 25.2% protein, 4.4% dietary fiber, 6.5% crude ash, 3.6% mineral mixture, 1% vitamin mixture, and 4% moisture. The HF diet study was carried out according to previously described methods (38, 39). The composition of the HF diet was 32% safflower oil, 33.1% casein, 17.6% sucrose, 5.6% cellulose, 9.8% mineral mixture, 1.4% vitamin mixture, and 0.5% DL-methionine.

In vivo glucose homeostasis. Glucose and insulin tolerance tests were performed as described previously (39, 40).

Histologic and immunohistochemical analysis and determination of adipocyte size. Adipose tissue was fixed with formaldehyde, and 10-μm sections were cut, mounted on glass slides, and stained with hematoxylin and eosin. White adipocyte areas were measured in 300 or more cells per mouse in each group, as described previously (39).

Immunohistochemical analysis of the endocrine pancreas and estimation of β cell and non–β cell mass and individual β cell size. Isolated pancreata were immersion-fixed in Bouin's solution at 4°C overnight. Tissue was then routinely processed for paraffin embedding, and 2-μm sections were cut and mounted on glass slides. The sections were double immunostained with guinea pig anti-porcine insulin antibody (diluted 1:200) and a cocktail composed of rabbit anti-porcine glucagon (diluted 1:200), rabbit anti-human somatostatin (diluted 1:800), and rabbit anti-human pancreatic polypeptide (diluted 1:800) antibodies (all from Dako). Images of pancreatic tissue, islet β cells, and islet non-β cells were captured on a computer through a microscope connected to a charge-coupled device camera (all from Olympus). The area of the β cells and non-β cells relative to the total area of pancreatic tissue was calculated with WinROOF software (version 5.0; Mitani Corp.) as described previously (41). More than 20 pancreatic sections from each animal, including representative sections of the head, body, and tail of the pancreas, were analyzed, and approximately 100 islets per mouse were counted in each group. Adjacent nonoverlapping fields were analyzed to obtain a true representation of average islet/β cell distribution throughout the pancreas. Individual β cell size was estimated by dividing the β cell area by the number of β cell nuclei in the area covered, as described previously (21). Maximum islet diameter was also calculated with WinROOF software. Immunostaining with anti-Ipf1 antibody (42) was performed as described previously (43). FoxO1 was immunohistochemically analyzed with anti-FoxO1 antibody (Cell Signaling Technology).

BrdU incorporation analysis and PCNA staining. BrdU incorporation was analyzed as described previously (44). In brief, BrdU (100 mg/kg in saline; Sigma-Aldrich) was intraperitoneally injected, and the pancreas was removed 6 hours later. The sections were double immunostained with anti-BrdU antibody (diluted 1:200; Dako) and a cocktail of anti-glucagon, anti-somatostatin, and anti-pancreatic polypeptide antibodies. BrdU-positive β cells were quantitatively assessed as a proportion of all β cells by counting the cells in approximately 50 islets per mouse. Sections were immunostained for PCNA with mouse anti-PCNA antibody (diluted 1:10; Progen Biotechnik) at 4°C for 48 hours.

Detection of apoptotic cells. Single-strand DNA analysis in islets was performed as described previously (45). Apoptotic cells were also detected in deparaffinized pancreatic sections by using an in situ cell death detection kit (Roche Diagnostics) according to the manufacturer's recommendations.

Islet isolation. For metabolic analysis, islets were isolated with collagenase as described previously (46). For preparation for RNA or protein, islets were isolated by using liberase RI (Roche Diagnostics) according to the manufacturer's instructions.

Analysis of insulin secretion and determination of glucose-phosphorylating activity, glucose oxidation, and cAMP content. Although the cellular composition of the islets may be affected by the dietary regimen, we used islets of comparable size (less than 250 μm in diameter) to assess islet insulin secretion and glucose metabolism, because quantitative determination of β cell mass in islets less than 250 μm in diameter yielded values in the 4 mouse groups that were indistinguishable. Insulin secretion by islets was analyzed as described previously (46). Glucose phosphorylation by hexokinase and Gck was assayed fluorometrically as described previously (3, 47). Hexokinase activity was measured at a glucose concentration of 0.5 mM, and the Gck activity was estimated as the difference between activity at 0.5 mM glucose and activity at 50 mM glucose. [U-^{14}C]glucose oxidation in mitochondria was assayed by measuring [^{14}C]CO_2 production as described previously (46). To extract cAMP for measurements, islet cells were disrupted by sonication for 5 seconds in 500 μl 95% ethanol at 4°C, vortexed vigorously, and centrifuged at 18,000 *g* for 30 minutes at 4°C. After removing the supernatant and evaporating to dryness, the samples were redissolved in sodium acetate buffer (0.05 mol/l, pH 6.2), and cAMP levels were determined with an enzyme-linked immunosorbent assay kit (cAMP Biotrak Enzymeimmunoassay System; Amersham Biosciences) in 96-well plates on a spectrophotometer at 450 nm according to the manufacturer's instructions.

Microarray analysis of mRNA levels in isolated islets. Isolated islets were cultured overnight in RPMI 1640 medium containing 11.1 mM glucose (Sigma-Aldrich) supplemented with 10% FBS, 0.075 g/l penicillin (Sigma-Aldrich),

and 0.1 g/l streptomycin (Sigma-Aldrich). Total RNA was isolated with the RNeasy Mini Kit (QIAGEN) and used as starting material for cDNA preparation. RNA was prepared from 7 mice of identical genotype. The first- and second-strand cDNA synthesis, array hybridization, and scanning were performed as described previously (48). In brief, RNA amplification was started with 5 μg of total islet RNA. Double-stranded cDNA was synthesized with the SuperScript Choice system (Gibco) and a T7-(dT) 24 Primer (Amersham Pharmacia Biotech). In vitro transcription was performed to produce biotin-labeled cRNA by using a BioArray HighYield RNA Transcript Labeling Kit (Affymetrix) according to the manufacturer's instructions. cRNA was linearly amplified approximately 40-fold with T7 polymerase by using half of the double-stranded cDNA that was synthesized. The readings obtained by quantitative scanning were analyzed with Affymetrix Gene Expression Analysis software. For expression change calls, we used the comparative analysis (Wilcoxon signed rank test–based analysis) program in Microarray Suite version 5.0 as described previously (49). The analysis was performed with the default parameters, where the P value of significant difference was below 0.0025.

Immunoblotting. The polyclonal anti-Irs1, anti-Irs2, and anti-p85 antibodies were purchased from Upstate USA Inc. The polyclonal anti-Insr antibody, and anti-Igf1rβ antibody were purchased from Santa Cruz Biotechnology Inc. The anti-Akt antibody, anti-Igf1rα antibody, anti-CREB antibody, and phospho-CREB (Ser133) antibody were purchased from Cell Signaling Technology Inc. The polyclonal anti-Ipf1 antibody (42) was provided by Y. Kajimoto (Osaka University, Suita, Japan). Islets were sonicated in ice-cold buffer A (25 mM Tris-HCl, pH 7.4, 10 mM Na_3VO_4, 10 mM NaPPi, 100 mM NaF, 10 mM EDTA, 10 mM EGTA, and 1 mM phenylmethylsulfonyl fluoride) with an ultrasonic sonicator. Samples were separated by SDS-polyacrylamide gel electrophoresis, and immunodetection was performed with an ECL kit (Amersham Biosciences). Protein was prepared from more than 100 islets pooled from several mice of identical genotype, and 20 μg samples of proteins were applied to the gel.

Statistics. Results are expressed as mean ± SEM. Statistical analysis was performed using the StatView software system (version 4.5; Abacus). Differences between 2 groups were analyzed for statistical significance by Student's t test for unpaired comparisons. Individual comparisons among more than 2 groups were assessed with the post-hoc Fisher's pairwise least-significant-difference test. A P value less than 0.05 was considered to be statistically significant.

Acknowledgments

We dedicate this paper to K. Komeda, who devoted his life to studying the pathophysiology of diabetes with animal models. We thank Y. Kajimoto for the generous gift of anti-Ipf1 antibody and Y. Meguro, E. Yoshida, A. Nagano, Y. Muto, M. Nakashima, N. Kowatari, and H. Chiyonobu for their excellent technical assistance and animal care. This work was supported by a grant for Life & Socio-Medical Science from the Kanae Foundation, a grant by the Tanabe Medical Frontier Conference, a Grant-in-Aid for Scientific Research in Priority Areas (B) 15390285 and (B) 16390263 from the Ministry of Education, Culture, Sports, Science and Technology of Japan, and a grant for the 2006 Strategic Research Project of Yokohama City University (to Y. Terauchi) as well as a Grant-in-Aid for Creative Scientific Research (10NP0201) from the Japan Society for the Promotion of Science, a Grant-in-Aid for Scientific Research in Priority Areas (C), a Grant-in-Aid for the Development of Innovative Technology from the Ministry of Education, Culture, Sports, Science and Technology of Japan, Health Science Research Grants (Research on the Human Genome and Gene Therapy) from the Ministry of Health and Welfare, a grant from the Program for Promotion of Fundamental Studies in Health Sciences of the Organization for Pharmaceutical Safety and Research of Japan, and a Grant-in-Aid (1-2000-231 and 1-2003-746) from the Juvenile Diabetes Research Foundation (to T. Kadowaki).

Received for publication December 17, 2002, and accepted in revised form November 7, 2006.

Address correspondence to: Takashi Kadowaki, Department of Metabolic Diseases, Graduate School of Medicine, University of Tokyo, 7-3-1 Hongo, Bunkyo-ku, Tokyo 113-8655, Japan. Phone: 81-3-5800-8815; Fax: 81-3-5800-9797; E-mail: kadowaki-3im@h.u-tokyo.ac.jp.

Yasuo Terauchi, Iseki Takamoto, and Naoto Kubota contributed equally to this work.

Kajuro Komeda is deceased.

1. Matschinsky, F.M., and Ellerman, J.E. 1968. Metabolism of glucose in the islets of Langerhans. *J. Biol. Chem.* **243**:2730–2736.
2. Velho, G., et al. 1997. Identification of 14 new glucokinase mutations and description of the clinical profile of 42 MODY-2 families. *Diabetologia.* **40**:217–224.
3. Terauchi, Y., et al. 1995. Pancreatic β-cell-specific targeted disruption of glucokinase gene. *J. Biol. Chem.* **270**:30253–30256.
4. Matschinsky, F.M. 1996. Banting Lecture 1995. A lesson in metabolic regulation inspired by the glucokinase glucose sensor paradigm. *Diabetes.* **45**:223–241.
5. Taylor, S.I., Accili, D., and Imai, Y. 1994. Insulin resistance or insulin deficiency: which is the primary cause of NIDDM? *Diabetes.* **43**:735–740.
6. Polonsky, K.S., Sturis, J., and Bell, G.I. 1996. Non-insulin-dependent diabetes mellitus-A genetically programmed failure of the beta cell to compensate for insulin resistance. *N. Engl. J. Med.* **334**:777–783.
7. Bonner-Weir, S. 2000. Postnatal pancreatic β cell growth. *Endocrinology.* **141**:1926–1929.
8. Tamemoto, H., et al. 1994. Insulin resistance and growth retardation in mice lacking insulin receptor substrate-1. *Nature.* **372**:182–186.
9. Araki, E., et al. 1994. Alternative pathway of insulin signaling in mice with targeted disruption of the IRS-1 gene. *Nature.* **372**:186–190.
10. Withers, D.J., et al. 1998. Disruption of IRS-2 causes type 2 diabetes in mice. *Nature.* **391**:900–904.
11. Kubota, N., et al. 2000. Disruption of insulin receptor substrate-2 causes type 2 diabetes due to liver insulin resistance and lack of compensatory β-cell hyperplasia. *Diabetes.* **49**:1880–1889.
12. Shulman, G.I. 2000. Cellular mechanisms of insulin resistance. *J. Clin. Invest.* **106**:171–176.
13. Yamauchi, T., et al. 2001. Replenishment of the fat-derived hormone adiponectin reverses insulin resistance in lipoatrophic diabetes and type 2 diabetes. *Nat. Med.* **7**:941–946.
14. Weisberg, S.P., et al. 2003. Obesity is associated with macrophage accumulation in adipose tissue. *J. Clin. Invest.* **112**:1796–1808. doi:10.1172/JCI200319246.
15. Kulkarni, R.N. 2005. New insights into the roles of insulin/IGF-I in the development and maintenance of β-cell mass. *Rev. Endocr. Metab. Disord.* **6**:199–210.
16. Rhodes, C.J. 2000. IGF-I and GH post-receptor signaling mechanisms for pancreatic β-cell replication. *J. Mol. Endocrinol.* **24**:303–311.
17. Ahlgren, U., Jonsson, J., Jonsson, L., Simu, K., and Edlund, H. 1998. Beta-cell-specific inactivation of the mouse Ipf1/Pdx1 gene results in loss of the beta-cell phenotype and maturity onset diabetes. *Genes Dev.* **12**:1763–1768.
18. Nakae, J., et al. 2002. Regulation of insulin action of pancreatic β-cell function by mutant alleles of the forkhead transcription factor Foxo1. *Nat. Genet.* **32**:245–253.
19. Ueki, K., et al. 2006. Total insulin and IGF-I resistance in pancreatic β cells cause overt diabetes. *Nat. Genet.* **38**:583–588.
20. Tuttle, R.L., et al. 2001. Regulation of pancreatic β-cell growth and survival by the serine/threonine protein kinase Akt1/PKBα. *Nat. Med.* **7**:1133–1137.
21. Bernal-Mizrachi, E., Wen, W., Stahlhut, S., Welling, C.M., and Permutt, M.A. 2001. Islet β cell expression of constitutively active Akt1/PKB α induces striking hypertrophy, hyperplasia, and hyperinsulinemia. *J. Clin. Invest.* **108**:1631–1638. doi:10.1172/JCI200113785.
22. Freemark, M., et al. 2002. Targeted deletion of the PRL receptor: effects on islet development, insulin production, and glucose tolerance. *Endocrinology.* **143**:1378–1385.
23. Garcia-Ocana, A., et al. 2000. Hepatocyte growth factor overexpression in the islet of transgenic mice increases beta cell proliferation, enhances islet mass, and induces mild hypoglycemia. *J. Biol. Chem.* **275**:1226–1232.
24. Aizawa, T., et al. 1996. Analysis of pancreatic β cell in the mouse with targeted disruption of the pan-

creatic β cell-specific glucokinase gene. *Biochem. Biophys. Res. Commun.* **229**:460–465.
25. Unger, R.H. 1995. Lipotoxicity in the pathogenesis of obesity-dependent NIDDM: genetic and clinical implications. *Diabetes.* **44**:863–870.
26. Mason, T.M., et al. 1999. Prolonged elevation of plasma free fatty acids desensitizes the insulin secretory response to glucose in vivo in rats. *Diabetes.* **48**:524–530.
27. Suzuki, R., et al. 2003. Pdx1 expression in Irs2 deficient mouse β-cells is regulated in a strain-dependent manner. *J. Biol. Chem.* **278**:43691–43698.
28. Jhala, U.S., et al. 2003. cAMP promotes pancreatic β-cell survival via CREB-mediated induction of IRS2. *Genes Dev.* **17**:1575–1580.
29. Ide, T., et al. 2004. SREBPs suppress IRS-2-mediated insulin signalling in the liver. *Nat. Cell Biol.* **6**:351–357.
30. Kitamura, T., et al. 2002. The forkhead transcription factor FoxO1 links insulin signaling to Pdx1 regulation of pancreatic β cell growth. *J. Clin. Invest.* **110**:1839–1847. doi:10.1172/JCI200216857.
31. Okamaoto, H., et al. 2006. Role of the forkhead protein FoxO1 in β cell proliferation to insulin resistance. *J. Clin. Invest.* **116**:775–782. doi:10.1172/JCI24967.
32. Shih, D.Q., et al. 2002. Profound defects in pancreatic β-cell function in mice with combined heterozygous mutations in Pdx-1, Hnf-1α, and Hnf-3β. *Proc. Natl. Acad. Sci. U. S. A.* **99**:3818–3823.
33. Hashimoto, N., et al. 2006. Ablation of PDK1 in pancreatic β cells induces diabetes as a result of loss of beta cell mass. *Nat. Genet.* **38**:589–593.
34. Fajans, S.S., Bell, G.I., and Polonsky, K.S. 2001. Molecular mechanisms and clinical pathophysiology of maturity-onset diabetes of the young. *N. Engl. J. Med.* **345**:971–980.
35. Stone, L.M., Kahn, S.E., Fujimoto, W.Y., Deeb, S.S., and Porte, D., Jr. 1996. A variation at position -30 of the beta-cell glucokinase gene promoter is associated with reduced beta-cell function in middle-aged Japanese-American men. *Diabetes.* **45**:422–428.
36. Katagiri, H., et al. 1992. Nonsense mutation of glucokinase gene in late-onset non-insulin-dependent diabetes mellitus. *Lancet.* **340**:1316–1317.
37. Rhodes, C.J. 2005. Type 2 diabetes-a matter of β-cell life and death? *Science.* **307**:380–384.
38. Ikemoto, S., et al. 1995. High fat diet-induced hyperglycemia: prevention by low level expression of a glucose transporter (GLUT4) minigene in transgenic mice. *Proc. Natl. Acad. Sci. U. S. A.* **92**:3096–3099.
39. Kubota, N., et al. 1999. PPARγ mediates high-fat diet-induced adipocyte hypertrophy and insulin resistance. *Mol. Cell.* **4**:597–609.
40. Terauchi, Y., et al. 1999. Increased insulin sensitivity and hypoglycaemia in mice lacking p85α subunit of phosphoinositide 3-kinase. *Nat. Genet.* **21**:230–235.
41. Terauchi, Y., et al. 1997. Development of non-insulin-dependent diabetes mellitus in the double knockout mice with disruption of insulin receptor substrate-1 and β-cell glucokinase genes. *J. Clin. Invest.* **99**:861–866.
42. Watada, H., et al. 1996. The human glucokinase gene β-cell-type promoter: an essential role of insulin promoter factor 1 (IPF1)/PDX-1 in its activation in HIT-T15 cells. *Diabetes.* **45**:1478–1488.
43. Kaneto, H., et al. 1999. Beneficial effects of antioxidants in diabetes. Possible protection of pancreatic β-cells against glucose toxicity. *Diabetes.* **48**:2398–2406.
44. Ishii, C., et al. 1996. Beta-cell replication in insulin-induced remission of IDDM in BB/Wor//Tky rats. *Diabetes Res.* **31**:1–18.
45. Kubota, N., et al. 2004. Insulin receptor substrate 2 plays a crucial role in β cells and the hypothalamus. *J. Clin. Invest.* **114**:917–927. doi:10.1172/JCI200421484.
46. Eto, K., et al. 1999. Role of NADH shuttle system in glucose-induced activation of mitochondrial metabolism and insulin secretion. *Science.* **283**:981–985.
47. Miwa, I., et al. 1995. Utility of 3-*O*-methyl-N-acetyl-D-glucosamine, an N-acetylglucosamine kinase inhibitor, for accurate assay of glucokinase in pancreatic islets and liver. *Enzyme Protein.* **48**:135–142.
48. Ishii, M., et al. 2000. Direct comparison of GeneChip and SAGE on the quantitative accuracy in the transcript profiling analysis. *Genomics.* **68**:136–143.
49. Liu, W.M., et al. 2002. Analysis of high density expression microarrays with signed-rank call algorithms. *Bioinformatics.* **18**:1593–1598.

ARTICLES

nature medicine

Targeted disruption of AdipoR1 and AdipoR2 causes abrogation of adiponectin binding and metabolic actions

Toshimasa Yamauchi[1–3,7], Yasunori Nio[1,2,7], Toshiyuki Maki[1,7], Masaki Kobayashi[1], Takeshi Takazawa[1], Masato Iwabu[1,2], Miki Okada-Iwabu[1,2], Sachiko Kawamoto[1], Naoto Kubota[1–3], Tetsuya Kubota[1], Yusuke Ito[1], Junji Kamon[1], Atsushi Tsuchida[1], Katsuyoshi Kumagai[1], Hideki Kozono[1], Yusuke Hada[1,3], Hitomi Ogata[4], Kumpei Tokuyama[4], Masaki Tsunoda[5], Tomohiro Ide[5], Kouji Murakami[5], Motoharu Awazawa[1,3], Iseki Takamoto[1–3], Philippe Froguel[6], Kazuo Hara[1,3], Kazuyuki Tobe[1,3], Ryozo Nagai[1], Kohjiro Ueki[1] & Takashi Kadowaki[1,3]

Adiponectin plays a central role as an antidiabetic and antiatherogenic adipokine. AdipoR1 and AdipoR2 serve as receptors for adiponectin *in vitro*, and their reduction in obesity seems to be correlated with reduced adiponectin sensitivity. Here we show that adenovirus-mediated expression of AdipoR1 and R2 in the liver of *Lepr*$^{-/-}$ mice increased AMP-activated protein kinase (AMPK) activation and peroxisome proliferator-activated receptor (PPAR)-α signaling pathways, respectively. Activation of AMPK reduced gluconeogenesis, whereas expression of the receptors in both cases increased fatty acid oxidation and lead to an amelioration of diabetes. Alternatively, targeted disruption of AdipoR1 resulted in the abrogation of adiponectin-induced AMPK activation, whereas that of AdipoR2 resulted in decreased activity of PPAR-α signaling pathways. Simultaneous disruption of both AdipoR1 and R2 abolished adiponectin binding and actions, resulting in increased tissue triglyceride content, inflammation and oxidative stress, and thus leading to insulin resistance and marked glucose intolerance. Therefore, AdipoR1 and R2 serve as the predominant receptors for adiponectin *in vivo* and play important roles in the regulation of glucose and lipid metabolism, inflammation and oxidative stress *in vivo*.

Adiponectin (also known as Acrp30)[1–4] is a hormone secreted by adipocytes that acts as a major antidiabetic and antiatherogenic adipokine. Plasma adiponectin levels are decreased in obesity, insulin resistance and type 2 diabetes[1–4]. Decreased adiponectin is implicated in the development of insulin resistance in obesity, which is reversed by the replenishment of adiponectin[5–7]. This insulin-sensitizing effect of adiponectin seems to be mediated by the inhibition of gluconeogenesis[7] and the stimulation of fatty acid oxidation[5,6] via activation of AMP-activated protein kinase (AMPK)[8,9] and peroxisome proliferator-activated receptor (PPAR)-α (refs. 10,11). Adiponectin also has antiatherogenic properties: for instance, it has anti-inflammatory effects in endothelial cells and macrophages[1–4].

We reported previously that AdipoR1 and R2 serve as receptors for adiponectin *in vitro*[12] and that their expression levels are reduced in obesity, apparently in correlation with reduced adiponectin sensitivity[13]. However, it remains to be clarified whether AdipoR1 and AdipoR2 serve as the major receptors for adiponectin, while also acting as key physiological regulators of glucose and lipid metabolism, *in vivo*.

We report here that adenovirus-mediated expression of either AdipoR1 or AdipoR2 in the liver ameliorated obesity-linked insulin resistance and diabetes. In contrast, simultaneous disruption of AdipoR1 and R2 abrogated adiponectin-specific binding and the glucose-lowering effect of adiponectin, and resulted in marked glucose intolerance and insulin resistance. We also demonstrate functional differences between AdipoR1 and AdipoR2 in adiponectin-signaling pathways: namely, that AdipoR1 may be more tightly linked to activation of AMPK pathways, whereas AdipoR2 seems to be associated with the activation of PPAR-α pathways and the inhibition of inflammation[14] and oxidative stress[15]. These data indicate that AdipoR1 and R2 serve as the physiologically most important receptors for adiponectin, while playing crucial roles in the regulation of glucose and lipid metabolism, as well as inflammation and oxidative stress, *in vivo*.

RESULTS

Adipor1 and r2 expression in *Lepr*$^{-/-}$ mice improves diabetes

Adipor mRNA levels are decreased in obesity[13], so we first examined the expression levels of *Adipor* mRNAs in the liver of *Lepr*$^{-/-}$ (also known as *db/db*) mice, a genetic animal model of human obesity. Expression levels of *Adipor1* and *Adipor2* decreased to approximately 65% and 55%, respectively, in the liver of *Lepr*$^{-/-}$ mice as compared with wild-type mice (**Fig. 1a**).

[1]Department of Internal Medicine, Graduate School of Medicine, University of Tokyo, Tokyo 113-8655, Japan. [2]Department of Integrated Molecular Science on Metabolic Diseases, 22nd Century Medical and Research Center, University of Tokyo, Tokyo 113-8655, Japan. [3]Core Research for Evolutional Science and Technology, Japan Science and Technology, Tokyo 332-0012, Japan. [4]Graduate School of Comprehensive Human Sciences, University of Tsukuba, Tsukuba 305-8577, Japan. [5]Bioscience Division I, Metabolic Discovery Research Laboratories, Kyorin Pharmaceutical Co. Ltd., Shimotsuga 329-0114, Japan. [6]Section of Genomic Medicine, Imperial College London, Hammersmith Hospital, Du Cane Road, London W12 ONN, UK. [7]These authors contributed equally to this work. Correspondence should be addressed to T.K. (kadowaki-3im@h.u-tokyo.ac.jp).

Received 19 December 2006; accepted 26 January 2007; published online 1 February 2006; doi:10.1038/nm1557

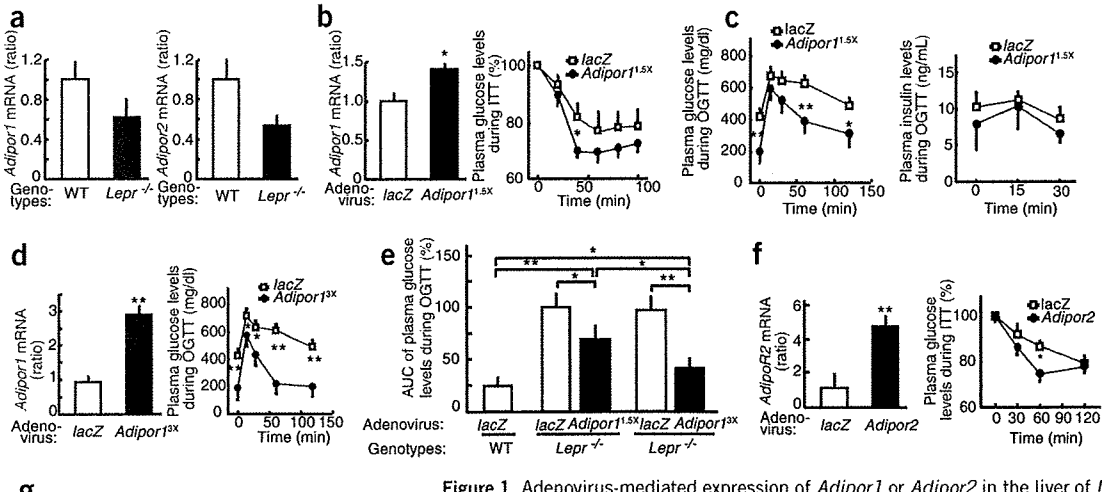

Figure 1 Adenovirus-mediated expression of *Adipor1* or *Adipor2* in the liver of *Lepr*$^{-/-}$ mice improves insulin resistance and ameliorates diabetes. (**a**–**g**) The amounts of *Adipor1* and *Adipor2* mRNA in the liver, plasma glucose levels, insulin levels and area under the curves (AUC) during the oral glucose tolerance test (OGTT) or the insulin tolerance test (ITT). We used wild-type C57Bl/6 (WT) and *Lepr*$^{-/-}$ mice. In addition, some mice were infected with an adenovirus expressing *lacZ*, *Adipor1* or *Adipor2*. Adenovirus concentrations used were 1.0×10^8(1.5X) and 3×10^8(3.0X) plaque-forming units (pfu) per gram body weight. Ratios in **a**,**b**,**d** and **f** are with respect to values of control mice. Percentages in **b** and **f** are with respect to values at time 0. Percentage in **e** is with respect to value of *lacZ*-infected *Lepr*$^{-/-}$ mice. Results indicate mean ± s.e.m. $n = 10$ for wild-type, untreated *Lepr*$^{-/-}$ and AdipoR2-infected *Lepr*$^{-/-}$ mice; 15 for *lacZ*- or R1$^{1.5\times}$-infected *Lepr*$^{-/-}$ mice; 11 for R1$^{3\times}$-infected *Lepr*$^{-/-}$ mice. #$P = 0.06$; *$P < 0.05$; **$P < 0.01$ (between two groups, as indicated, or versus *lacZ*).

To determine how decreased expression of *Adipor* mRNA is involved in the development of insulin resistance and diabetes in obese mice, we next studied the effects of restoring *Adipor1* expression, by means of an adenovirus, in *Lepr*$^{-/-}$ mice. Following injection of the adenovirus, *Adipor1* expression levels were increased 1.5-fold in the liver of *Lepr*$^{-/-}$ mice (**Fig. 1b**), comparable to levels in the wild-type mice (**Fig. 1a**), which did indeed significantly improve insulin resistance (**Fig. 1b**) and diabetes (**Fig. 1c**). However, this improvement was only partial, though significant ($P < 0.01$), since the area under the curve (AUC, a measure of plasma glucose levels during the oral glucose tolerance test) decreased to 74% in *Lepr*$^{-/-}$ mice, compared to an AUC of 24% in the wild-type mice (**Fig. 1e**). This improvement in diabetes occurred without an increase in plasma insulin levels (**Fig. 1c**). These data suggest that insulin resistance and diabetes in *Lepr*$^{-/-}$ mice are presumably caused, at least in part, by decreases in *Adipor1*. This notion is further supported by the data showing that even further overexpression of *Adipor1* in the liver of *Lepr*$^{-/-}$ mice (3-fold, **Fig. 1d**) now markedly ameliorated diabetes (**Fig. 1d**), indicating an expression level–dependent improvement (**Fig. 1e** and **Supplementary Fig. 1** online). Likewise, adenovirus-mediated 5-fold overexpression of *Adipor2* in the liver of *Lepr*$^{-/-}$ mice (**Fig. 1f**) markedly improved insulin resistance (**Fig. 1f**) and ameliorated diabetes (**Fig. 1g**), and was associated with a decrease in plasma insulin levels (**Fig. 1g**).

The effects of the adenovirus-mediated 1.5-fold expression of *Adipor1* or 5-fold overexpression of *Adipor2* in the liver on the amelioration of diabetes were lost in adiponectin-deficient[16–19] *Lepr*$^{-/-}$ mice (**Supplementary Fig. 1**). These data are consistent with our conclusion that the phenotypes resulting from restoration of adiponectin receptors in the liver are due to increased adiponectin signaling.

To identify the physiological mechanisms involved in the amelioration of diabetes seen in our earlier results, we performed a hyperinsulinemic euglycemic clamp experiment (**Fig. 2a**). Adenovirus-mediated restoration of *Adipor1* significantly reduced endogenous glucose production (EGP), whereas overexpression of *Adipor2* had little effect on EGP (**Fig. 2a**). However, both adenovirus-mediated restoration of *Adipor1* and overexpression of *Adipor2* increased the glucose infusion rate (GIR) by about 2-fold (**Fig. 2a**), indicating increased insulin sensitivity.

To further examine the role of *Adipor1* or *Adipor2* in the regulation of gluconeogenesis, we performed a pyruvate challenge test[20] by investigating the rise in plasma glucose in response to the administration of pyruvate, a precursor for gluconeogenesis[20]. Adenovirus-mediated restoration of *Adipor1* significantly suppressed the rise in plasma glucose concentration after pyruvate injection (**Fig. 2b**), whereas overexpression of *Adipor2* had little effect (**Fig. 2b**).

AdipoR1 increases AMPK activation by adiponectin in liver

We next studied whether adenovirus-mediated expression of *Adipor1* or *Adipor2* in the liver of *Lepr*$^{-/-}$ mice increases the effects of adiponectin, such as the activation of AMPK (refs. 8,9) and PPAR-α (refs. 10,11). Adenovirus-mediated restoration of AdipoR1 resulted in significantly increased activation of AMPK in the liver by adiponectin (**Fig. 2c**), whereas overexpression of *Adipor2* did not (**Fig. 2d**). These results suggested that *Adipor1* may be more involved in the activation of AMPK by adiponectin than *Adipor2* in the liver *in vivo*.

The activation of AMPK in the liver has been reported to reduce the expression of genes encoding hepatic gluconeogenic enzymes such as glucose-6-phosphatase (*G6pc*) and phosphoenolpyruvate carboxykinase 1 (*Pck1*)[21], as well as that of genes encoding molecules involved in lipogenesis, such as sterol regulatory element-binding protein 1c (*Srebf1*)[22]. As predicted by these earlier studies, we found that adenovirus-mediated restoration of *Adipor1* significantly decreased the expressions of *G6pc* (**Fig. 2e**), *Pck1* (**Fig. 2f**) and *Srebf1* (**Fig. 2g**) in the liver of *Lepr*$^{-/-}$ mice; this may be a possible mechanism by which the restoration of *Adipor1* in the liver reduced EGP (**Fig. 2a**), while

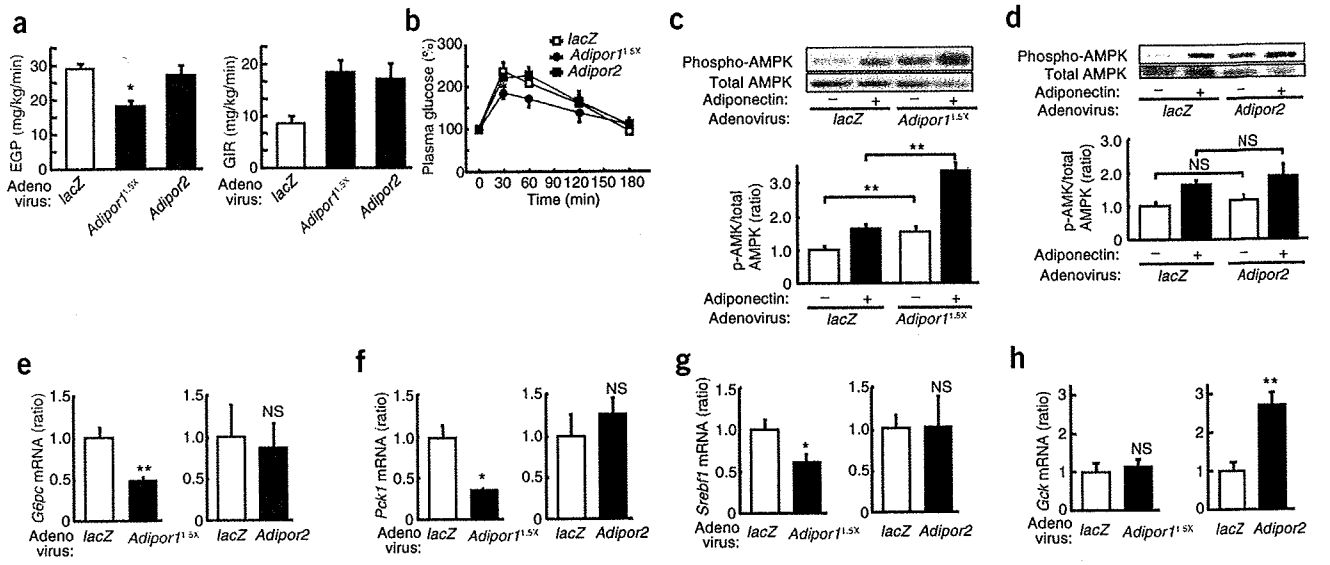

Figure 2 Adenovirus-mediated expression of AdipoR1 in the liver of *Lepr*$^{-/-}$ mice results in activation of AMP kinase pathways. (**a**) Endogenous glucose production (EGP) and glucose infusion rate (GIR) during hyperinsulinemic euglycemic clamp. (**b**) Plasma glucose levels during pyruvate challenge test. (**c**,**d**) Phosphorylation and amount of AMPK after treatment with or without full-length adiponectin (30 μg per 10 g body weight) for 10 min. (**e**–**h**) Amounts of *G6pc*, *Pck1*, *Srebf1* and *Gck* mRNA in the liver of *Lepr*$^{-/-}$ mice infected with an adenovirus expressing *lacZ*, *Adipor1*$^{1.5\times}$ or *Adipor2*. Percentage in **b** is with respect to value at time 0. Ratios in **c**–**h** are with respect to values in *lacZ*-infected mice. Densitometric quantification of bands is shown in **c** and **d**.; data were corrected for the total amount of AMPK protein in each sample and are expressed as the ratio to the value of vehicle-injected mice infected with adenoviruses expressing *lacZ*. Data are represented as mean ± s.e.m. $n = 7$–12 in **b**,**e**–**h**; 5–7 in **a**,**c**,**d** (per condition). $^*P < 0.05$; $^{**}P < 0.01$; NS, no significant difference (between two groups, as indicated, or versus *lacZ*).

increasing the GIR (**Fig. 2a**) and improving diabetes (**Fig. 1e**). In contrast, overexpression of *Adipor2* had little effect on the expression levels of *G6pc* (**Fig. 2e**), *Pck1* (**Fig. 2f**) or *Srebf1* (**Fig. 2g**).

AdipoR2 increases PPAR-α target genes in liver

Although *Adipor2* overexpression had no effect on the gene expression of proteins involved in gluconeogenesis, it did significantly increase the expression of a gene involved in glucose uptake (glucokinase (*Gck*)[23]), whereas restoration of *Adipor1* did not (**Fig. 2h**). Thus, whereas both *Adipor1* restoration and *Adipor2* overexpression increase the GIR (**Fig. 2a**) and ameliorate diabetes (**Fig. 1c**,**g**) they appear to do so by effects on different aspects of glucose metabolism.

Adenovirus-mediated expression of *Adipor2* in the liver of *Lepr*$^{-/-}$ mice increased the expression of the gene encoding PPAR-α itself (*Ppara*; **Fig. 3a**) and its target genes[10], including *Acox1* (encoding acyl-CoA oxidase; **Fig. 3b**) and *Ucp2* (encoding uncoupling protein 2; **Fig. 3b**). In contrast, adenovirus-mediated expression of *Adipor1* had little effect on any of these genes (**Fig. 3a**,**b**). These observations suggested that AdipoR2 may be more involved in the activation of the PPAR-α pathways than AdipoR1. Because both AMPK (ref. 24) and PPAR-α (ref. 10) have been reported to increase fatty acid oxidation, we next examined the effects of adenovirus-mediated expression of *Adipor1* and *Adipor2* on fatty acid oxidation and tissue triglyceride content[25]. We noted a significant increase in the former (**Fig. 3c**) and a decrease in

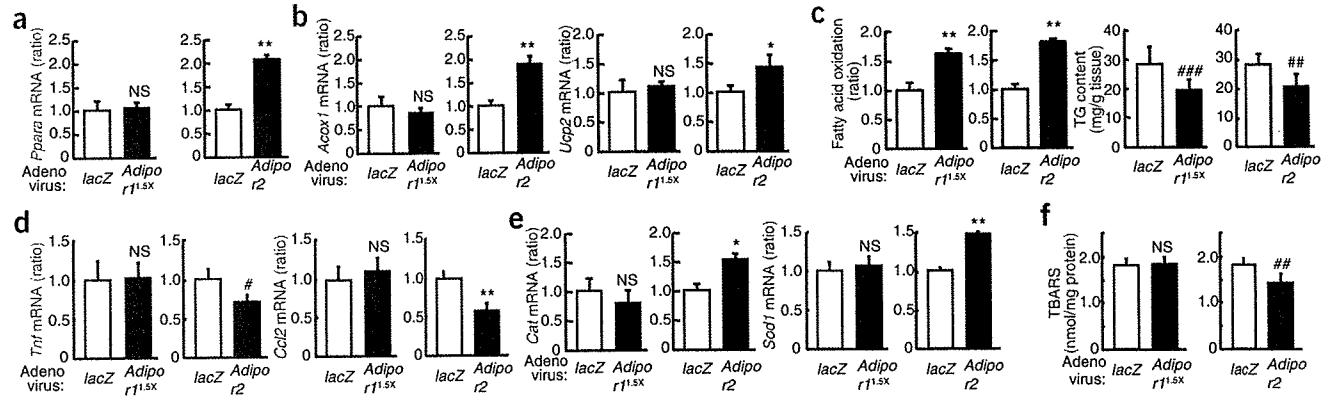

Figure 3 Adenovirus-mediated expression of *Adipor2* in the liver of *Lepr*$^{-/-}$ mice results in activation of PPAR-α pathways. (**a**,**b**) Amounts of *Ppara*, *Acox1* and *Ucp2* mRNA in the liver. (**c**) Extent of fatty acid oxidation and triglyceride content in the liver. (**d**,**e**) Amount of *Tnf* and *Ccl2*, and *Cat* and *Sod1* mRNA in the liver. (**f**) Thiobarbituric acid reactive substance (TBARS) in the liver. *Lepr*$^{-/-}$ mice were infected with an adenovirus expressing *lacZ*, *Adipor1*$^{1.5\times}$ or *Adipor2*. Ratios in **a**–**e** are with respect to values in *lacZ*-infected mice. Data are represented as mean ± s.e.m. $n = 7$–10 per condition. $^*P < 0.05$; $^{**}P < 0.01$; NS, no significant difference; $^{\#\#\#}P = 0.09$ (in **c**); $^{\#}P = 0.12$ (in **d**); $^{\#\#}P = 0.11$ (in **c**,**f**).

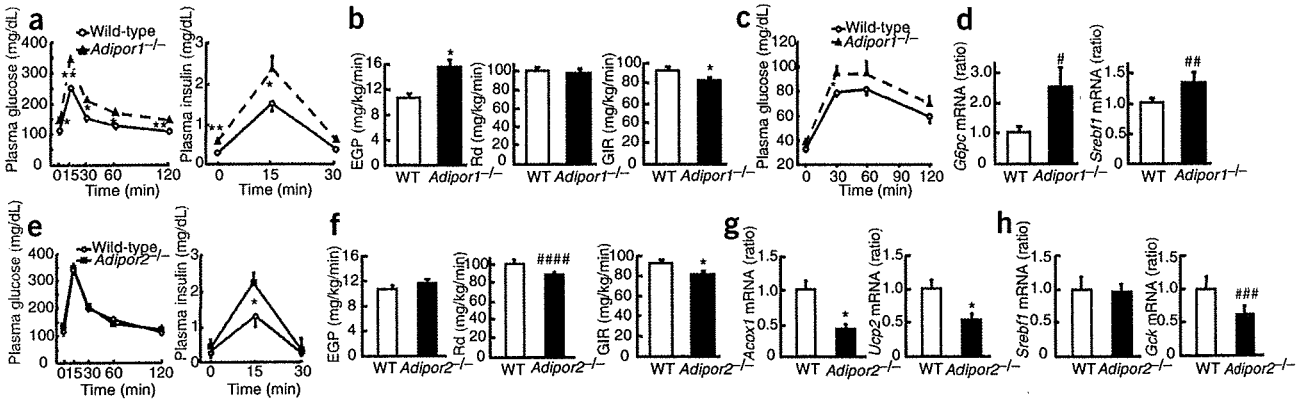

Figure 4 Targeted disruption of *Adipor1* results in increased glucose production, whereas that of *Adipor2* results in decreased glucose uptake. (**a**) Plasma glucose and plasma insulin in wild-type (WT) and *Adipor1*$^{-/-}$ mice during OGTT (2 g glucose per kg body weight). (**b**) Endogenous glucose production (EGP), rates of glucose disposal (Rd) and glucose infusion rate (GIR) in wild-type and *Adipor1*$^{-/-}$ mice during hyperinsulinemic euglycemic clamp study. (**c**) Plasma glucose in wild-type and *Adipor1*$^{-/-}$ mice during pyruvate challenge test. (**d**) Amounts of *G6pc* and *Srebf1* mRNA in liver from wild-type and *Adipor1*$^{-/-}$ mice. (**e**) As in **a** but for in wild-type and *Adipor2*$^{-/-}$ mice. (**f**) As in **b** but for wild-type and *Adipor2*$^{-/-}$ mice. (**g**) Amounts of *Acox1* and *Upc2* mRNA in liver from wild-type and *Adipor2*$^{-/-}$ mice. (**h**) Amounts of *Srebf1* and *Gck* mRNA in liver from wild-type and *Adipor2*$^{-/-}$ mice. Mice used were from a C57Bl/6 background. Data were obtained during (**b**,**f**) or after (**d**,**g**,**h**) the hyperinsulinemic euglycemic clamp studies. Results are stated as mean ± s.e.m. $n = 10$–16 per genotype. $^{*}P < 0.05$; $^{**}P < 0.01$; $\#P = 0.16$ and $\#\#P = 0.15$ (in **d**); $\#\#\#\#P = 0.07$ (in **f**); $\#\#\#P = 0.13$ (in **h**).

the latter (**Fig. 3c**) as a result of the adenovirus-mediated expression of either *Adipor1* or *Adipor2* in the liver of *Lepr*$^{-/-}$ mice.

Proinflammatory cytokines such as tumor necrosis factor (TNF)-α (ref. 26) and chemokines[14] such as monocyte chemoattractant protein (MCP)-1 (refs. 27–30) are involved in the induction of insulin resistance in obesity, whereas PPAR-α has been reported to reduce it[31–33]. Oxidative stress[15] is also involved in the induction of insulin resistance[34,35], and PPAR-α increases the expression of molecules involved in the reduction of oxidative stress, such as catalase[36] and Cu,Zn-superoxide dismutase (SOD1)[37], whose promoters contain peroxisome proliferator response elements (PPRE). Adenovirus-mediated expression of *Adipor2* in the liver of *Lepr*$^{-/-}$ mice increased *Ppara* (**Fig. 3a**), reduced *Tnf* and *Ccl2* (the gene encoding MCP-1, also known as chemokine (C-C motif) ligand 2; **Fig. 3d**), and significantly increased catalase (*Cat*) and *Sod1* (**Fig. 3e**), while reducing oxidative stress (**Fig. 3f**). In contrast, adenovirus-mediated expression of *Adipor1* had no statistically significant effects on these

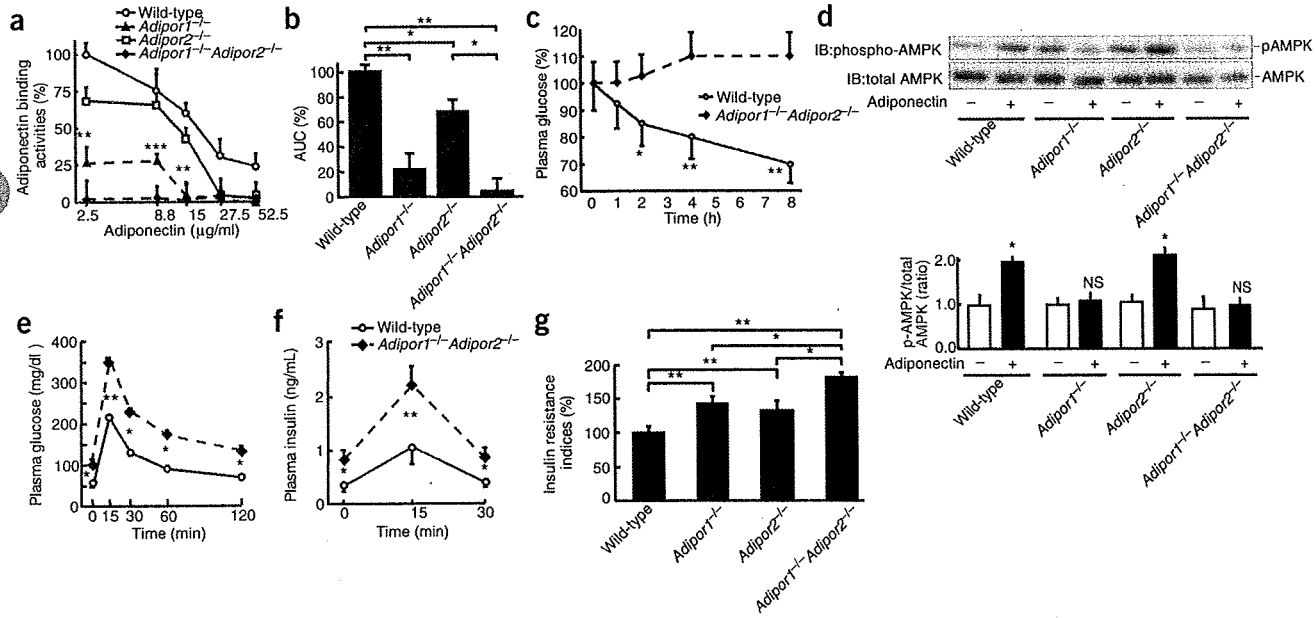

Figure 5 Targeted disruption of both *Adipor1* and *Adipor2* results in abrogation of adiponectin binding and adiponectin actions, leading to marked glucose intolerance and insulin resistance. (**a**,**b**) Binding and AUC of binding of full-length adiponectin to the primary hepatocytes. (**c**) Plasma glucose during the adiponectin sensitivity test (30 μg per 10 g body weight). (**d**) Phosphorylation and amount of AMPK in liver treated with or without full-length adiponectin (30 μg per 10 g body weight) for 10 min. (**e**,**f**) Plasma glucose and plasma insulin during the oral glucose tolerance test. (**g**) Insulin resistance indices. Mice were on a C57Bl/6 and 129/sv background. Percentages in **a** and **b** are with respect to the values in wild-type mice. Percentage in **c** is with respect to value at time 0. Densitometric quantification of bands is shown in **d**; data were corrected for the total amount of AMPK protein in each sample and are expressed as a ratio of the values in vehicle-injected wild-type mice. Results are represented as mean ± s.e.m. $n = 6$ in **a**,**b** and **d**; 10 in **c**; 20 in **e** and **f**; and 10-20 in **g** (per genotype or condition). $^{*}P < 0.05$; $^{**}P < 0.01$; $^{***}P = 0.06$; NS, no significant difference (between two groups, as indicated, or versus wild-type, or versus vehicle).

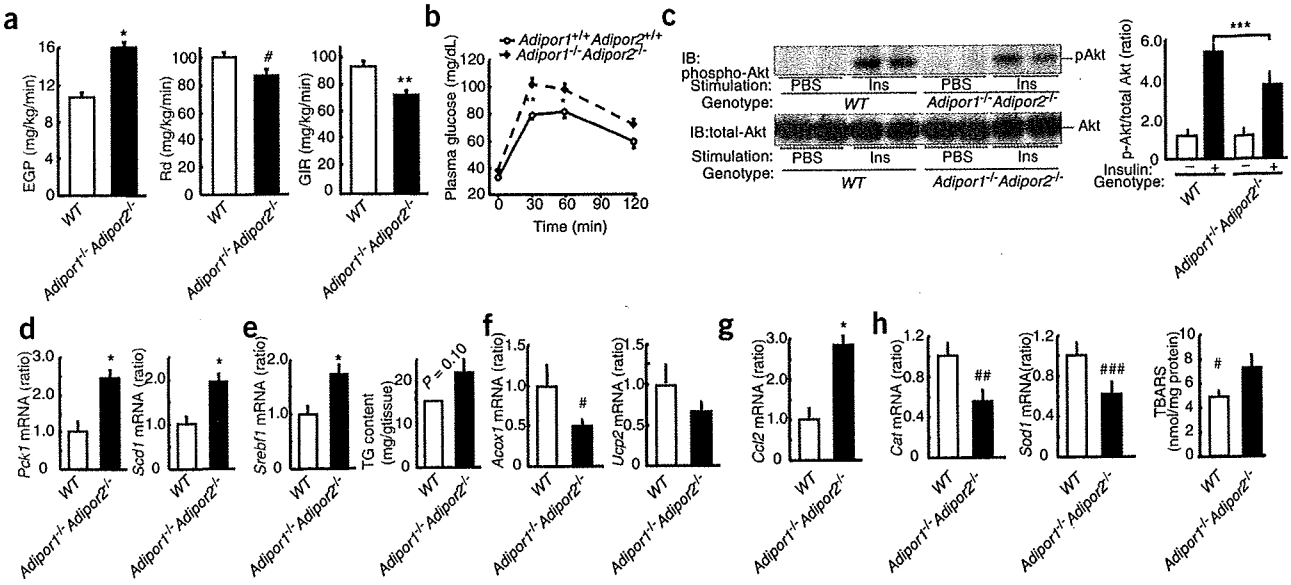

Figure 6 Targeted disruption of both *Adipor1* and *Adipor2* results in dysregulation of AMPK and PPAR-α pathways, leading to increased EGP and decreased GIR. (**a**) Endogenous glucose production (EGP), rates of glucose disposal (Rd) and glucose infusion rate (GIR) during hyperinsulinemic euglycemic clamp study. WT; wild-type (**b**) Plasma glucose levels during the pyruvate challenge test. (**c**) Phosphorylation and amount of Akt treated with or without insulin (0.01 U per g body weight) for 10 min. (**d**) Amounts of *Pck1* and *Scd1* mRNA. (**e**) Amount of *Srebf1* mRNA and triglyceride content. (**f**) Amounts of *Acox1* and *Ucp2* mRNA. (**g**) Amount of *Ccl2* mRNA. (**h**) Amounts of *Cat* and *Sod1* mRNA, and TBARS. Data in **c**–**e** are from the liver; in **f**, from skeletal muscle; and in **g** and **h**, from white adipose tissue. Mice were on a C57Bl/6 and 129/sv background. Results in **c**–**h** are with respect to values in vehicle control (**c**) or wild type (**d**–**h**). Densitometric quantification of bands is shown in **c**; data were corrected for the total amount of Akt protein in each sample and are expressed as a ratio of the values in vehicle-injected wild-type mice. Results are represented as mean ± s.e.m. $n = 10$ per genotype in **a** and **b**; 4–7 per genotype or condition in **c**–**h**. $^{*}P < 0.05$; $^{**}P < 0.01$; $^{***}P = 0.07$; $\#P = 0.08$ (in **f** and **h**); $\#\#P = 0.10$, $\#\#\#P = 0.06$ (in **h**) (between two groups, as indicated, or versus wild type).

parameters (**Fig. 3a,d–f**). The reduction of inflammation and oxidative stress (**Fig. 3d–f**) also seemed to be among possible mechanisms by which overexpression of *Adipor2* in the liver improved insulin resistance (**Fig. 1f,g** and **Fig. 2a**).

Adipor1-KO mice show increased EGP and insulin resistance

We generated *Adipor1*-knockout mice, confirmed by Southern blot analysis (**Supplementary Fig. 2** online). Northern blot analysis and real-time PCR revealed an approximate 50% reduction of *Adipor1* mRNA expression in the liver of heterozygous *Adipor1*-knockout mice (**Supplementary Fig. 2**) and the abrogation of *Adipor1* mRNA expression in the liver, skeletal muscle and white adipose tissue of homozygous *Adipor1*-knockout mice (**Supplementary Figs. 2** and **3** online).

Adipor1-knockout mice were viable and fertile, with normal body weight, and developed normally. Growth curves were similar to those of wild-type mice until at least 1 year of age, and food intake was normal (data not shown). Plasma glucose and insulin levels in fed mice were significantly higher in *Adipor1*-knockout mice relative to control wild-type mice (**Supplementary Fig. 4** online). To assess glucose metabolism in the former group, we performed an oral glucose tolerance test (**Fig. 4a**). *Adipor1*-knockout mice showed significantly impaired glucose tolerance (**Fig. 4a**) and significantly higher plasma insulin concentrations as compared to those in control wild-type mice, indicating that they had developed insulin resistance (**Fig. 4a**). EGP was significantly increased and GIR significantly decreased in *Adipor1*-knockout mice as compared to control wild-type mice (**Fig. 4b**), indicating increased hepatic glucose production and insulin resistance in the former group. Moreover, the pyruvate-induced rise in plasma glucose concentration was significantly increased in *Adipor1*-knockout mice (**Fig. 4c**), suggesting that AdipoR1 is required for the proper regulation of gluconeogenesis. Hepatic *G6pc* expression levels were higher in *Adipor1*-knockout mice than in wild-type mice (**Fig. 4d**), which is consistent with the increased hepatic glucose production in the former (**Fig. 4b**). Hepatic *Srebf1* expression levels were also higher in the knockouts (**Fig. 4d**), consistent with the idea that AdipoR1 is the physiological link between activation of AMPK and adiponectin signaling (**Fig. 2c**).

Adipor2-KO mice show insulin resistance

We also generated *Adipor2*-knockout mice (**Supplementary Figs. 2** and **3**), which were carried to term. Although these mice expressed a small amount of an aberrantly spliced *Adipor2* mRNA, this mRNA could not make a protein (**Supplementary Fig. 2** and **Supplementary Note** online).

Adipor2-knockout mice were viable and fertile (both males and females). Disruption of *Adipor2* did not change body weight. Although glucose intolerance was not observed in these mice (**Fig. 4e**), their plasma insulin levels were significantly higher than in the wild-type mice (**Fig. 4e**), suggesting that they had developed insulin resistance. In contrast to our finding in *Adipor1*-knockout mice, EGP was not significantly higher in *Adipor2*-knockout mice (**Fig. 4f**). However, GIR and glucose disposal were both decreased in these mice (**Fig. 4f**).

To clarify the molecular mechanisms by which AdipoR2 deficiency decreased GIR, we studied the expression levels of molecules involved in glucose metabolism and insulin sensitivity. Hepatic expression levels of PPAR-α target genes, such as *Acox1* (**Fig. 4g**) and *Ucp2* (**Fig. 4g**), were significantly decreased and hepatic *Gck* expression levels slightly decreased (**Fig. 4h**) in *Adipor2*-knockout mice, which may have contributed to decreased GIR in these mice.

Adipor1/r2 KO abrogates adiponectin binding and actions

We also generated *Adipor1/r2* double-knockout mice (**Supplementary Figs. 2** and **3**), which were carried to term. These mice were viable and fertile (both males and females). Simultaneous disruption of *Adipor1* and *Adipor2* did not change body weight.

First, we studied whether adiponectin could specifically bind to primary hepatocytes, a major target of adiponectin action[6,7,19], obtained from each knockout mouse (**Fig. 5a,b**). Specific adiponectin binding to hepatocytes from *Adipor1*-knockout mice was markedly decreased (**Fig. 5a,b**) and that in *Adipor2*-knockout mice was slightly, but significantly, decreased (as assessed by comparing the AUC of binding activities; **Fig. 5b**). Notably, we detected no appreciable adiponectin-specific binding activity in the hepatocytes from *Adipor1/r2* double-knockout mice (**Fig. 5a,b**), indicating undetectable levels of functional adiponectin receptors in hepatocytes from these mice.

We next studied the action of adiponectin in *Adipor1/r2* double-knockout mice. We have previously reported that treating wild-type mice with adiponectin reduces plasma glucose levels and that this was at least partly due to decreased gluconeogenesis resulting from AMPK activation[8]. Here, we found that treatment of wild-type mice with adiponectin significantly reduced plasma glucose levels (**Fig. 5c**), whereas this effect was completely abolished in *Adipor1/r2* double-knockout mice (**Fig. 5c**). These data indicate that AdipoR1 and AdipoR2 serve as the major physiological adiponectin receptors *in vivo*.

Next we examined the role of AdipoR1 and AdipoR2 in adiponectin-induced AMPK activation in the liver *in vivo* (**Fig. 5d**) and in hepatocytes *ex vivo* (**Supplementary Fig. 4**). Adiponectin increased the phosphorylation of AMPK in the liver *in vivo* and in hepatocytes *ex vivo* isolated from wild-type littermates and *Adipor2*-knockout mice but not in those from *Adipor1*-knockout mice and *Adipor1/r2* double-knockout mice (**Fig. 5d** and **Supplementary Fig. 4**). These results demonstrate that AdipoR1, but not AdipoR2, is required for adiponectin-mediated activation of AMPK in the liver.

Adipor1/r2 KO results in marked glucose intolerance

We next studied glucose metabolism in *Adipor1/r2* double-knockout mice. These mice showed markedly impaired glucose tolerance (**Fig. 5e**). Their plasma insulin concentrations were significantly higher than those of control wild-type mice (**Fig. 5f**), indicating that *Adipor1/r2* double-knockout mice exhibit insulin resistance. There was a significant elevation of the insulin resistance index in the double knockouts compared to the *Adipor1*-knockout mice (**Fig. 5g**); this can be attributed to the *Adipor2* deficiency (**Fig. 5g**).

We next performed the oral glucose tolerance test on mice fed a high-fat diet (**Supplementary Fig. 4**). *Adipor1*-knockout, *Adipor2*-knockout and *Adipor1/r2* double-knockout mice exhibited significantly impaired glucose tolerance and increasing plasma insulin levels on a high-fat diet (**Supplementary Fig. 4**), indicating development of insulin resistance and glucose intolerance on this diet.

Adipor1/r2 double-knockout mice showed significantly increased EGP, decreased glucose disposal and significantly decreased GIR (**Fig. 6a**). These observations indicate increased hepatic glucose production and insulin resistance in the liver and potentially decreased glucose uptake and mild insulin resistance in the skeletal muscle. Moreover, the pyruvate-induced rise in plasma glucose concentration was significantly increased compared to wild-type (**Fig. 6b**), almost as much as in *Adipor1* knockout mice (**Fig. 4c**), suggesting that AdipoR1 is required for proper regulation of gluconeogenesis.

In the liver of *Adipor1/r2* double-knockout mice, insulin receptor and insulin receptor substrate(IRS)-2 tyrosine phosphorylation (**Supplementary Fig. 4**) and insulin-stimulated Akt phosphorylation (**Fig. 6c**) were decreased as compared to that in wild-type mice, suggesting insulin resistance in the liver of the double-knockout.

We next studied the expression levels of molecules involved in glucose and lipid metabolism. Simultaneous disruption of both *Adipor1* and *Adipor2* significantly increased the expression levels of genes encoding molecules involved in gluconeogenesis, such as *Pck1* (**Fig. 6d**), which may explain the increased EGP in this strain (**Fig. 6a**). Moreover, simultaneous disruption of both *Adipor1* and *Adipor2* significantly increased the expression levels of genes encoding molecules involved in fatty acid synthesis, such as *Scd1* (ref. 38 and **Fig. 6d**) and *Srebf1* (**Fig. 6e**), while also increasing tissue triglyceride content in the liver (**Fig. 6e**) and decreasing the expression of genes encoding molecules involved in fatty acid oxidation, such as *Acox1* (**Fig. 6f**), and energy expenditure, such as *Ucp2*, in muscle (**Fig. 6f**).

As we had determined for the individual overexpressors of *Adipor1* and *Adipor2*, we examined inflammation and oxidative stress in adipose tissue[39] from knockout mice. Simultaneous disruption of *Adipor1* and *Adipor2* resulted in significantly increased expression of genes encoding chemokines, such as *Ccl2* (**Fig. 6g**), and decreased expression of genes encoding molecules that reduce oxidative stress, such as *Cat* and *Sod1* (**Fig. 6h**), and increased oxidative stress in white adipose tissue (**Fig. 6h**).

Discussion

In this study, we found that expression of *Adipor1* or *Adipor2* in liver can reverse insulin resistance and diabetes in the *db/db* (*Lepr*$^{-/-}$) mouse model of obesity and type 2 diabetes. The present data suggest that downregulation of *Adipor1* and *Adipor2* in obesity are involved in the development of insulin resistance and diabetes.

We showed the apparent functional differences between AdipoR1 and AdipoR2 in adiponectin signaling pathways. AdipoR1 was more tightly linked to the activation of the AMPK pathways which regulate the inhibition of gluconeogenesis and thus may be associated with the decreased EGP observed in *Lepr*$^{-/-}$ mice overexpressing *Adipor1* in the liver. In contrast, AdipoR2 was more involved with activation of the PPAR-α pathways, which stimulate energy dissipation and inhibit inflammation and oxidative stress, and thus may be associated with the increased GIR seen in *Lepr*$^{-/-}$ mice overexpressing *Adipor2* in the liver. Stimulation of fatty acid oxidation by the expression of *Adipor1* and *Adipor2* may be mediated via the AMPK and PPAR-α pathways, respectively, which in turn lead to decreased triglyceride content. Thus, both pathways can increase insulin sensitivity though by different signaling mechanisms. These functional differences between AdipoR1 and AdipoR2 may be accounted for by AdipoR1- or AdipoR2-specific intracellular binding proteins. We are attempting to identify such proteins, which may mediate the activation of AMPK and PPAR-α, respectively, by adiponectin.

In *Adipor1/r2* double-knockout mice, adiponectin-specific binding and adiponectin-induced actions, such as reductions in serum glucose levels, were abrogated. Thus AdipoR1 and AdipoR2 are the major physiological receptors for adiponectin, while mediating most, if not all, parts of adiponectin binding and adiponectin actions *in vivo*. Although T-cadherin[40], which is also expressed in the liver, is reported to be capable of binding to adiponectin, we found that simultaneous disruption of *Adipor1* and *Adipor2* was sufficient to almost completely abolish adiponectin binding to the liver, which is the major organ responsible for mediating the whole-body metabolic effects generated by adiponectin[6,7,19]. Not surprisingly then, the *Adipor1/r2* double-knockout also completely abolished the major adiponectin-induced metabolic effects (such as decreases in serum glucose levels). Thus, it remains to be determined whether T-cadherin is a physiologically relevant receptor, although it may bind adiponectin *in vivo*.

Targeted disruption of either *Adipor1* or *Adipor2* resulted in insulin resistance, and disruption of both resulted in a marked glucose intolerance and insulin resistance. These findings provide the first direct evidence, to our knowledge, that AdipoR1 and AdipoR2 do indeed play important physiological roles in the regulation of insulin sensitivity *in vivo*. However, the observation that the *Adipor1/r2* double-knockout mice appeared to be more insulin resistant and glucose intolerant than the adiponectin-knockout mice raises a few possibilities that we are currently investigating. Namely, there may be other ligands for AdipoR1/AdipoR2 in addition to adiponectin, and AdipoR1 and/or AdipoR2 may have basal constitutive activities.

The insulin resistance in *Adipor1*-knockout mice was manifested in the significant increase in gluconeogenic enzymes, increased EGP and greatly increased plasma glucose during pyruvate challenge tests, which could be accounted for by the abrogation of adiponectin-induced AMPK activation in the liver. In contrast, insulin resistance in *Adipor2*-knockout mice was characterized by the significantly decreased GIR and tendency for decreased glucose disposal, which may have resulted from decreased glucose uptake in the liver and possibly also in the skeletal muscle. It is possible that the decreased glucose uptake in the liver of these mice resulted from a decrease in the number of molecules involved in glucose uptake (such as glucokinase) and/or from a decrease in PPAR-α activation in the liver. It is unlikely that the insulin resistance in the *Adipor1* knockout is due to similar effects because we did not observe decreased PPAR-α activation or decreased glucokinase in that mutant nor was the glucose disposal rate changed. However, we cannot account for the decreased glucose uptake in the skeletal muscle of *Adipor2*-knockout mice by decreased AMPK activation in skeletal muscle because the AMPK pathway does not appear to be regulated by AdipoR2. Indeed, abrogation of adiponectin-induced AMPK activation in muscle was not observed in the *Adipor2*-knockout mice, although it was seen in *Adipor1*-knockout mice (**Supplementary Fig. 5** online). Instead, it may have been due to decreased PPAR-α activation in the skeletal muscle, indirect actions of decreased PPAR-α activation in the liver, increased inflammation, increased oxidative stress in WAT or all of the above. We did not observe any of these alterations in *Adipor1*-knockout mice. To determine the magnitude of insulin resistance and the role of AdipoR2 in skeletal muscle, experiments such as tracer studies, *ex vivo* studies in muscle strips or studies using labeled 2-deoxyglucose injections *in vivo* will be informative and will be the subject of future experiments.

Adipor1/r2 double-knockout mice exhibited the phenotypes of both *Adipor1*-knockout mice and *Adipor2*-knockout mice. Thus they showed significantly increased EGP, decreased glucose disposal and greatly decreased GIR. Both the increase in EGP and the decrease in glucose disposal may be accounted for by *Adipor1* deficiency, which also decreases AMPK activation and increases the levels of gluconeogenic enzymes and increases the rise in plasma glucose during pyruvate challenge test, whereas the *Adipor2* deficiency decreases PPAR-α activation and increases inflammation and oxidative stress. The marked decrease in GIR may be caused by both increased EGP and decreased glucose disposal.

Although relying on different signaling pathways (that is, AMPK and PPAR-α), a common end point (increased fatty acid oxidation and reduced triglyceride content) may be how the expression of either *Adipor1* or *Adipor2* in the liver could improve insulin resistance and diabetes. The reduction of inflammation and oxidative stress also seemed to be among possible mechanisms by which overexpression of *Adipor2* in the liver improved insulin resistance. Moreover, we noted an increase in oxidative stress in white adipose tissue (WAT), which may be one of the mechanisms by which simultaneous disruption of *Adipor1* and *Adipor2* results in marked glucose intolerance, insulin resistance, significantly decreased GIR and slightly decreased glucose disposal.

In conclusion, AdipoR1 and AdipoR2 are key players in the physiological and pathophysiological significance of adiponectin, and are involved in the regulation of glucose and lipid metabolism, inflammation and oxidative stress. This study suggests that agonism of AdipoR1/R2, as well as strategies to increase AdipoR1/R2, may be logical approaches to providing a new treatment modality for insulin resistance and type 2 diabetes linked to obesity.

METHODS

Generation of *Adipor1*- and *Adipor2*-knockout mice. To construct the targeting vector for disruption of the *Adipor1* or *Adipor2* gene, a neomycin resistance gene was substituted for exons 2, 3 and 4 of the *Adipor1* gene or exon 3 of the *Adipor2* gene (**Supplementary Fig. 2**). The strategy for culturing, electroporation of J1 embryonic stem (ES) cells (129/Sv), and screening for homologous recombinant clones was as described previously[16], with slight modifications. Male chimeric mice were mated with C57Bl/6 female mice to generate heterozygous offspring, and F1 progeny from two independently generated male chimeric mice were crossed to obtain F2 mice. Both mice lines showed identical phenotypes in all experiments carried out in this study. *Adipor1*$^{-/-}$/*Adipor2*$^{-/-}$ mice were prepared by *Adipor1*$^{+/-}$/*Adipor2*$^{+/-}$ mouse intercrosses (**Figs. 5** and **6**, and **Supplementary Figs. 2–5**). All experiments in this study were conducted on male littermates. The procedures used for Southern blot analysis have been described previously[16].

Mice. Mice were 8–10 weeks of age at the time of the experiment. They were housed in cages and maintained on a 12-h light-dark cycle. For the experiment depicted in **Supplementary Figure 4**, we used high-fat diet 32 consisting of 25.5% (wt/wt) protein, 2.9% fiber, 4.0% ash, 29.4% carbohydrates, 32% fat and 6.2% water (CLEA Japan Inc.)[30]. For all other experiments, the diets were standard chow (CE-2, CLEA Japan Inc.) with the following composition: 25.6% (wt/wt) protein, 3.8% fiber, 6.9% ash, 50.5% carbohydrates, 4% fat and 9.2% water[18]. Male *Lepr*$^{-/-}$ or C57Bl/6 mice (aged 8–10 weeks) were purchased from Japan CLEA. To study AMPK phosphorylation *in vivo*, we injected 30 μg recombinant murine adiponectin per 10 g body weight intravenously in mice through an inferior vena cava catheter[8]. This resulted in an increase of plasma adiponectin levels, to approximately 30 μg/ml; this showed that the adiponectin dose used in this study was comparable to endogenous adiponectin levels. Mouse full-length adiponectin was generated as previously described[6,8,12]. The glucose tolerance, insulin tolerance and adiponectin sensitivity tests were conducted as previously described[6,8], with slight modifications. For the pyruvate challenge test[20], mice deprived of food overnight were injected intraperitoneally with pyruvate dissolved in saline (2 g/kg). Plasma glucose concentration was measured at the indicated times thereafter. The pyruvate-induced increase in plasma glucose concentration was abolished by previous administration of 3-mercaptopicolinic acid (30 mg/kg), an inhibitor of gluconeogenesis (data not shown), suggesting that this effect of pyruvate was dependent on gluconeogenesis. The animal care and use procedures were approved by the Animal Care Committee of the University of Tokyo.

Northern blot analysis, quantitative analysis by real-time PCR and immunoblotting. Total RNA was prepared from cells or tissues with Trizol (Invitrogen) according to the manufacturer's instructions. We used a real-time PCR method to quantify the mRNAs (ref. 12), with slight modifications (**Supplementary Methods** online). Northern blot analysis was performed as described previously[12,16], with slight modifications. The procedures used for immunoblotting have been described previously[8,18,30]. The livers or muscles were freeze-clamped in liquid nitrogen *in situ*[8,18,30]. Phosphorylation and the protein levels of Akt and AMPKα were determined as described elsewhere[8,18,30]. Representative data from one of two or three independent experiments are shown.

Blood sample assays. Plasma glucose levels were determined using a glucose B-test (Wako Pure Chemical Industries). Plasma insulin was measured with an insulin immunoassay (Shibayagi). Plasma adiponectin levels were determined using a mouse adiponectin ELISA kit (Otsuka Pharmaceutical Co. Ltd.).

Adenovirus-mediated gene transfer *in vivo*. The recombinant adenoviruses Adex1CAAdipoR1 and Adex1CAAdipoR2 were constructed by homologous recombination between the expression cosmid cassette and the parental virus

genome[8]. Mice were injected intravenously with adenoviruses expressing *lacZ*, *Adipor1* (ref. 12) or *Adipor2* (ref. 12), at concentrations of 1×10^8 or 3×10^8 plaque-forming units (pfu) per gram of body weight, as previously described[8]. After 5–7 d, the mice were subjected to an overnight fast before testing. There were no significant differences between the livers from mice injected with adenoviruses expressing *lacZ*, *Adipor1* or *Adipor2*, in terms of the expression levels of housekeeping genes we examined.

Hyperinsulinemic-euglycemic clamp study. Clamp studies were carried out as described previously[18,30], with slight modifications (**Supplementary Methods**).

Mice primary hepatocytes. Hepatocytes were isolated from 8-week-old male mice by the collagenase perfusion method[13], with slight modifications (**Supplementary Methods**).

Binding assay. Recombinant full-length adiponectin was labeled with ^{125}I at Tyr by IODObeads (Pierce) in the presence of Na[^{125}I] (2,000 Ci/mmol, Amersham Pharmacia Biotech) according to the manufacturer's protocol. Binding assay was carried out as described previously[8,12], with slight modifications (**Supplementary Methods**).

Lipid metabolism, lipid peroxidation, and other materials. The measurements of [^{14}C]CO_2 production from [1-^{14}C]palmitic acid were performed using liver slices, as described elsewhere[6,8,11]. Liver homogenates were extracted, and tissue triglyceride content was determined as described previously[6,8,11], with some modifications. To investigate whether oxidative stress was increased, we measured lipid peroxidation, a marker of oxidative injury, represented by plasma thiobarbituric acid reactive substance (TBARS) as described[39]. Briefly, tissue samples were homogenized in a buffer solution containing 50 mM Tris-HCl (pH 7.4) and 1.15% KCl, and then centrifuged. The supernatant was used for the assay. The levels of lipid peroxidation in tissue homogenate were measured in terms of the amount of TBARS using the LPO test (Wako Pure Chemical Industries). All other materials, including chemicals, were from the sources given in refs. 6,8,12,13,18 and 30.

Statistical analysis. Results are expressed as the mean ± s.e.m. Differences between two groups were assessed using unpaired two-tailed *t*-tests. Data involving more than two groups were assessed by analysis of variance (ANOVA).

Note: Supplementary information is available on the Nature Medicine website.

ACKNOWLEDGMENTS

We thank K. Kangawa, M. Yanagisawa, K. Nakao, M. Kasuga, T. Shimizu, T. Yokomizo, W. Ogawa, H. Watada, Y. Terauchi, I. Manabe, M. Yamaguchi, K. Kobayashi and Y. Iwata for advice and discussions. We are grateful to A. Okano, A. Itoh and K. Miyata for technical assistance. This work was supported by a grant from the Program for Promotion of Fundamental Studies in Health Sciences of the Organization for Pharmaceutical Safety and Research of Japan (to T.K.), a grant-in-aid for the Development of Innovative Technology from the Ministry of Education, Culture, Sports, Science and Technology (to T. K.) and Health Science Research Grants (Research on Human Genome and Gene Therapy) from the Ministry of Health, Labour and Welfare (to T. K. and T.Y.).

COMPETING INTERESTS STATEMENT

The authors declare that they have no competing financial interests.

Published online at http://www.nature.com/naturemedicine
Reprints and permissions information is available online at http://npg.nature.com/reprintsandpermissions/

1. Hug, C. & Lodish, H.F. The role of the adipocyte hormone adiponectin in cardiovascular disease. *Curr. Opin. Pharmacol.* **5**, 129–134 (2005).
2. Scherer, P.E. Adipose tissue: from lipid storage compartment to endocrine organ. *Diabetes* **55**, 1537–1545 (2006).
3. Matsuzawa, Y. The metabolic syndrome and adipocytokines. *FEBS Lett.* **580**, 2917–2921 (2006).
4. Kadowaki, T. *et al.* Adiponectin and adiponectin receptors in insulin resistance, diabetes, and the metabolic syndrome. *J. Clin. Invest.* **116**, 1784–1792 (2006).
5. Fruebis, J. *et al.* Proteolytic cleavage product of 30-kDa adipocyte complement-related protein increases fatty acid oxidation in muscle and causes weight loss in mice. *Proc. Natl. Acad. Sci. USA* **98**, 2005–2010 (2001).
6. Yamauchi, T. *et al.* The fat-derived hormone adiponectin reverses insulin resistance associated with both lipoatrophy and obesity. *Nat. Med.* **7**, 941–946 (2001).
7. Berg, A.H., Combs, T.P., Du, X., Brownlee, M. & Scherer, P.E. The adipocyte-secreted protein Acrp30 enhances hepatic insulin action. *Nat. Med.* **7**, 947–953 (2001).
8. Yamauchi, T. *et al.* Adiponectin stimulates glucose utilization and fatty-acid oxidation by activating AMP-activated protein kinase. *Nat. Med.* **8**, 1288–1295 (2002).
9. Tomas, E. *et al.* Enhanced muscle fat oxidation and glucose transport by ACRP30 globular domain: acetyl-CoA carboxylase inhibition and AMP-activated protein kinase activation. *Proc. Natl. Acad. Sci. USA* **99**, 16309–16313 (2002).
10. Kersten, S., Desvergne, B. & Wahli, W. Roles of PPARs in health and disease. *Nature* **405**, 421–424 (2000).
11. Yamauchi, T. *et al.* Globular adiponectin protected ob/ob mice from diabetes and apoE deficient mice from atherosclerosis. *J. Biol. Chem.* **278**, 2461–2468 (2003).
12. Yamauchi, T. *et al.* Cloning of adiponectin receptors that mediate antidiabetic metabolic effects. *Nature* **423**, 762–769 (2003).
13. Tsuchida, A. *et al.* Insulin/Foxo1 pathway regulates expression levels of adiponectin receptors and adiponectin sensitivity. *J. Biol. Chem.* **279**, 30817–30822 (2004).
14. Wellen, K.E. & Hotamisligil, G.S. Inflammation, stress, and diabetes. *J. Clin. Invest.* **115**, 1111–1119 (2005).
15. Brownlee, M. Biochemistry and molecular cell biology of diabetic complications. *Nature* **414**, 813–820 (2001).
16. Kubota, N. *et al.* Disruption of adiponectin causes insulin resistance and neointimal formation. *J. Biol. Chem.* **277**, 25863–25866 (2002).
17. Maeda, N. *et al.* Diet-induced insulin resistance in mice lacking adiponectin/ACRP30. *Nat. Med.* **8**, 731–737 (2002).
18. Kubota, N. *et al.* Pioglitazone ameliorates insulin resistance and diabetes by both adiponectin-dependent and -independent pathways. *J. Biol. Chem.* **281**, 8748–8755 (2006).
19. Nawrocki, A.R. *et al.* Mice lacking adiponectin show decreased hepatic insulin sensitivity and reduced responsiveness to peroxisome proliferator-activated receptor gamma agonists. *J. Biol. Chem.* **281**, 2654–2660 (2006).
20. Miyake, K. *et al.* Hyperinsulinemia, glucose intolerance, and dyslipidemia induced by acute inhibition of phosphoinositide 3-kinase signaling in the liver. *J. Clin. Invest.* **110**, 1483–1491 (2002).
21. Lochhead, P.A., Salt, I.P., Walker, K.S., Hardie, D.G. & Sutherland, C. 5-aminoimidazole-4-carboxamide riboside mimics the effects of insulin on the expression of the 2 key gluconeogenic genes PEPCK and glucose-6-phosphatase. *Diabetes* **49**, 896–903 (2000).
22. Woods, A. *et al.* Characterization of the role of AMP-activated protein kinase in the regulation of glucose-activated gene expression using constitutively active and dominant negative forms of the kinase. *Mol. Cell. Biol.* **20**, 6704–6711 (2000).
23. Matschinsky, F.M. *et al.* The network of glucokinase-expressing cells in glucose homeostasis and the potential of glucokinase activators for diabetes therapy. *Diabetes* **55**, 1–12 (2006).
24. Long, Y.C. & Zierath, J.R. AMP-activated protein kinase signaling in metabolic regulation. *J. Clin. Invest.* **116**, 1776–1783 (2006).
25. Shulman, G.I. Cellular mechanisms of insulin resistance. *J. Clin. Invest.* **106**, 171–176 (2000).
26. Hotamisligil, G.S., Shargill, N.S. & Spiegelman, B.M. Adipose expression of tumor necrosis factor-alpha: direct role in obesity-linked insulin resistance. *Science* **259**, 87–91 (1993).
27. Weisberg, S.P. *et al.* Obesity is associated with macrophage accumulation in adipose tissue. *J. Clin. Invest.* **112**, 1796–1808 (2003).
28. Xu, H. *et al.* Chronic inflammation in fat plays a crucial role in the development of obesity-related insulin resistance. *J. Clin. Invest.* **112**, 1821–1830 (2003).
29. Kanda, H. *et al.* MCP-1 contributes to macrophage infiltration into adipose tissue, insulin resistance, and hepatic steatosis in obesity. *J. Clin. Invest.* **116**, 1494–1505 (2006).
30. Kamei, N. *et al.* Overexpression of MCP-1 in adipose tissues causes macrophage recruitment and insulin resistance. *J. Biol. Chem.* **281**, 26602–26614 (2006).
31. Staels, B. *et al.* Activation of human aortic smooth-muscle cells is inhibited by PPARα but not by PPARγ activators. *Nature* **393**, 790–793 (1998).
32. Delerive, P. *et al.* Peroxisome proliferator-activated receptor α negatively regulates the vascular inflammatory gene response by negative cross-talk with transcription factors NF-κB and AP-1. *J. Biol. Chem.* **274**, 32048–32054 (1999).
33. Tsuchida, A. *et al.* Peroxisome proliferator-activated receptor (PPAR)α activation increases adiponectin receptors and reduces obesity-related inflammation in adipose tissue: comparison of activation of PPARα, PPARγ and their combination. *Diabetes* **54**, 3358–3370 (2005).
34. Maddux, B.A. *et al.* Protection against oxidative stress-induced insulin resistance in rat L6 muscle cells by micromolar concentrations of α-lipoic acid. *Diabetes* **50**, 404–410 (2001).
35. Rudich, A. *et al.* Prolonged oxidative stress impairs insulin-induced GLUT4 translocation in 3T3-L1 adipocytes. *Diabetes* **47**, 1562–1569 (1998).
36. Toyama, T. *et al.* PPARalpha ligands activate antioxidant enzymes and suppress hepatic fibrosis in rats. *Biochem. Biophys. Res. Commun.* **324**, 697–704 (2004).
37. Inoue, I. *et al.* The ligands/activators for peroxisome proliferator-activated receptor alpha (PPARalpha) and PPARgamma increase Cu^{2+},Zn^{2+}-superoxide dismutase and decrease p22phox message expressions in primary endothelial cells. *Metabolism* **50**, 3–11 (2001).
38. Cohen, P. *et al.* Role for stearoyl-CoA desaturase-1 in leptin-mediated weight loss. *Science* **297**, 240–243 (2002).
39. Furukawa, S. *et al.* Increased oxidative stress in obesity and its impact on metabolic syndrome. *J. Clin. Invest.* **114**, 1752–1761 (2004).
40. Hug, C. *et al.* T-cadherin is a receptor for hexameric and high-molecular-weight forms of Acrp30/adiponectin. *Proc. Natl. Acad. Sci. USA* **101**, 10308–10313 (2004).

Technical Briefs

Improved ELISA for Selective Measurement of Adiponectin Multimers and Identification of Adiponectin in Human Cerebrospinal Fluid, *Hiroyuki Ebinuma,[1] Takashi Miida,[2]* Toshimasa Yamauchi,[3] Yusuke Hada,[3] Kazuo Hara,[3] Naoto Kubota,[3] and Takashi Kadowaki[3]* ([1] Diagnostics Research Laboratories, Daiichi Pure Chemicals Co. Ltd., Ibaraki, Japan; [2] Division of Clinical Preventive Medicine, Department of Community Preventive Medicine, Niigata University Graduate School of Medical and Dental Sciences, Niigata, Japan; [3] Department of Metabolic Diseases, Graduate School of Medicine, University of Tokyo, Tokyo, Japan; * address correspondence to this author at: Division of Clinical Preventive Medicine, Department of Community Preventive Medicine, Niigata University Graduate School of Medical and Dental Sciences, Asahimachi 1-757, Chuo-ku, Niigata, Niigata 951-8510, Japan; fax 81-25-223-0996, e-mail: miida@med.niigata-u.ac.jp)

Background: **Human serum adiponectin exists in 3 multimer forms: high molecular weight (HMW), middle molecular weight, and low molecular weight (LMW), with some of the latter bound to albumin (Alb)-LMW. Some studies have suggested that adiponectin crosses the blood–brain barrier and plays a central role in energy homeostasis.**

Methods: **To determine cerebrospinal fluid (CSF) adiponectin at extremely low concentrations, we modified the protocol of the ELISA system used to assay serum adiponectin. The 3 multimers of adiponectin were measured separately by pretreating CSF with 2 proteases. We measured the CSF adiponectin concentrations in anonymous human samples (n = 19). The molecular sizes of adiponectin in CSF pretreated with proteases or untreated were determined by use of native PAGE and immunoblotting.**

Results: **The ELISA system measured adiponectin in the range of 1.0–167 μg/L. The between-assay imprecision estimates (CVs) were 6%–17% for the 3 forms. The mean total CSF adiponectin concentration (7.2 μg/L) was ~1/1000 of the mean concentration in serum. Unlike serum adiponectin, the LMW and Alb-LMW forms predominated in all of the CSF samples. Immunoblotting analysis revealed that most LMW forms were bound to Alb, although the HMW form was detected in some samples.**

Conclusions: **The modified ELISA system measures the 3 multimers separately and is sufficiently sensitive to measure adiponectin in CSF.**

Adiponectin is an adipocyte-derived adipokine *(1)* with multiple functions, including antidiabetic *(2)*, antiatherogenic *(3)*, and antiinflammatory actions. Although the adiponectin target organs are the liver, muscles, and blood vessels, some studies have suggested that adiponectin has central effects on energy homeostasis. The intracerebroventricular administration of adiponectin in normal mice led to dose-dependent decreases in the body weight without substantial inhibition of food intake. Furthermore, intravenous adiponectin injection induced a >3-fold increase in cerebrospinal fluid (CSF) adiponectin concentration *(4)*. In contrast, a study of humans revealed that the adiponectin concentration in CSF made up only 0.1% of the serum adiponectin concentration, suggesting that adiponectin does not cross the blood–brain barrier *(5)*. Hence, controversy remains as to whether adiponectin can cross the blood–brain barrier under physiological conditions.

Adiponectin in human blood exists as 3 multimers with distinct molecular sizes: trimeric low molecular weight (LMW), hexameric middle molecular weight (MMW), and high molecular weight (HMW) forms *(6)*. Some of the LMW adiponectin exists as albumin (Alb)-bound forms (Alb-LMW) *(7)*. The molecular weights of adiponectin affect the strength of their metabolic actions. Several studies have suggested that HMW adiponectin and the ratio of HMW adiponectin to total adiponectin are more closely associated with insulin sensitivity and metabolic syndrome than is total adiponectin *(8, 9)*. ELISAs for measuring the 3 multimers separately *(10)* are available in Asia (Daiichi Pure Chemicals), the US, and the European Union (ALPCO Diagnostics).

We developed and tested a highly sensitive ELISA system for measuring CSF adiponectin and examined whether HMW adiponectin is detectable in human CSF. To measure extremely low concentrations of adiponectin in CSF, we modified the protocol of the ELISA used to measure serum adiponectin *(10)*. Human CSF was obtained from residual clinical samples that had normal cell counts and CSF concentrations of total protein, Alb, IgG, β_2-macroglobulin, glucose, lactate dehydrogenase, and chloride. We excluded samples in which erythrocyte contamination was detected by microscopic examination. After ensuring confidentiality of the identities of the sample donors, their CSF samples were labeled only with age and sex and were sent to our laboratory. To ensure that the samples were not contaminated with erythrocytes, we examined all of the CSF samples after low-speed centrifugation. Finally, we obtained 19 CSF samples [9 males and 10 females; mean (SD) age 51.6 (17.2) years] and stored them in a deep-freezer until use. Informed consent was obtained from all of the study participants, and the procedures were strictly in accordance with the statement of the Japanese Society of Laboratory Medicine on the use of residual clinical samples *(11)*.

This modified ELISA system enabled us to measure the 3 multimers separately by pretreating the samples with 2 proteases. A total of 150 μL of CSF is required to measure the concentrations of total adiponectin and all 3 multimers. To determine total adiponectin, we mixed 50 μL of CSF with 50 μL of pretreatment buffer containing no protease [50 mmol/L Tris-HCl (pH 8.0)]. The mixture was added to 50 μL of sample buffer [100 mmol/L sodium citrate (pH 3.0) containing 20 g/L sodium dodecyl sulfate

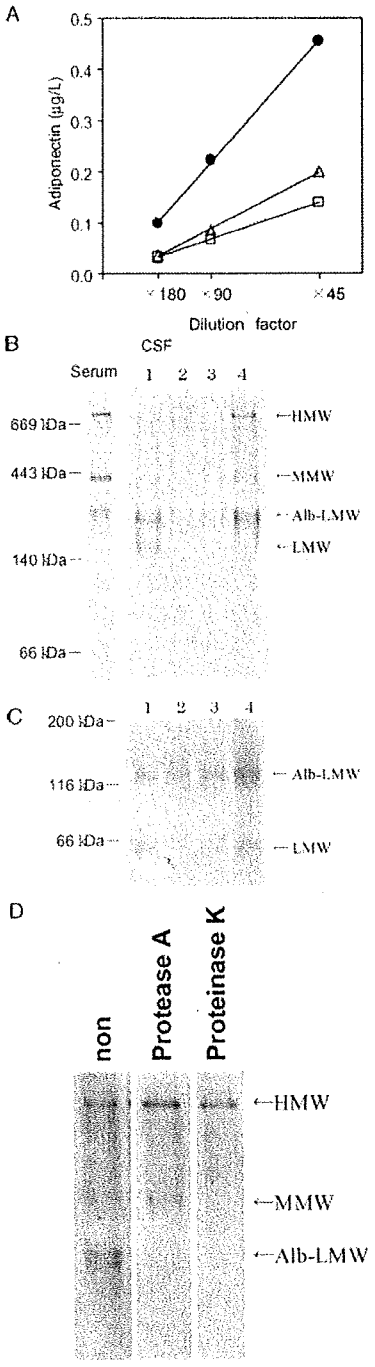

Fig. 1. Detection and quantification of adiponectin multimers in human CSF.

(*A*), linearity of the dilution curves of human CSF samples. After the 3 human CSF samples (Table 1, sample nos. 1–3) were treated according to the sample pretreatment procedure outlined for the total adiponectin assay, the samples were further diluted serially with BSA-PBST. (*B*), typical Western blotting analysis of adiponectin multimers in human CSF. Human CSF (4 μL; sample nos. 1–4) was separated using native PAGE and analyzed with Western blotting. (*C*), detection of the LMW form of adiponectin. Human CSF (1.0 μL; sample nos. 1–4) was separated using nonheating SDS-PAGE and analyzed with Western blotting. (*D*), selectivity of protease digestion. After human CSF (sample no. 4) was treated with protease A Amano or proteinase K according to the sample pretreatment procedure (without sample buffer), 4 μL each of the pretreated samples were separated using native PAGE and analyzed with Western blotting.

(SDS)]. For selective MMW + HMW adiponectin determination, 50 μL of CSF was incubated with the pretreatment buffer containing 1.0 g/L protease A Amano (Amano Enzyme) for 20 min at 37 °C. The mixture was then added to 50 μL of the sample buffer. For selective HMW adiponectin determination, we incubated 50 μL of CSF with the pretreatment buffer containing 3.75 kU/L of proteinase K (Roche Diagnostics) for 20 min at 37 °C. The mixture was then added to 50 μL of the sample buffer.

These pretreated samples were further diluted 31-fold with PBS (15 mmol/L, pH 7.5) containing 10 g/L BSA and 0.5 g/L Tween 20 (BSA-PBST). Each well of the polystyrene microtiter plates (Nunc) was coated with 50 μL of antihuman adiponectin monoclonal antibody (No. 64405; 5 mg/L in PBS) *(10)* and incubated overnight at 4 °C. After PBST rinsing, the wells were blocked with 100 μL of BSA-PBST at room temperature for 2 h. The calibrators (0–1.8 μg/L dimeric adiponectin from human serum) *(10)* or diluted samples (50 μL each) were placed in the wells and incubated at room temperature for 2 h. After rinsing with PBST, 50 μL of antihuman adiponectin biotinylated monoclonal antibody (No. 64404) *(10)* was added to each well, and the plate was incubated at room temperature for 1 h. After PBST rinsing, the biotinylated antibody was allowed to react with horseradish peroxidase–conjugated streptavidin (Pierce) at room temperature for 30 min. The trapped adiponectin–antibody complexes were then washed extensively and incubated with substrate solution (*o*-phenylenediamine in citrate buffer, pH 5.0, containing hydrogen peroxide) at room temperature for 20 min; the absorbance was measured at 492 nm. The concentrations of MMW and LMW (including Alb-LMW) adiponectin were obtained by subtracting the HMW concentration from the MMW + HMW concentrations and the MMW + HMW concentrations from the total adiponectin concentration, respectively. In the modified ELISA, the analytical limit of detection *(12)* was ~1.0 μg/L, and the calibration curve was linear up to 167 μg/L ($y = 1.10x + 0.14$, $r = 0.999$). Decreasing the sample dilution and increasing the sample incubation and substrate reaction times rendered this modified system ~200 times more sensitive than the original system used to measure serum adiponectin. We confirmed that the curve of measured values of serially diluted CSF samples paralleled the calibration curve (Fig. 1A). The intraassay CVs (n = 8) were 7.3% and 2.7% at adiponectin concentrations of 7.1 and 17.8 μg/L, respectively. The interassay CVs (n = 4) were 6.3%, 17.2%, and 5.8% for the total adiponectin, MMW + HMW, and HMW assays, respectively, at adiponectin concentrations of 19.0 μg/L.

Despite the extremely low CSF-adiponectin concentrations, we measured adiponectin successfully in 19 clinical samples (Table 1). The mean (SD) total CSF adiponectin concentration was 7.2 (7.2) μg/L, which is ~1000 times lower than the serum adiponectin concentration. We also used electrophoresis to quantify the total adiponectin

concentrations. The adiponectin multimers were converted into the dimer by heat denaturation and subjected to SDS-PAGE. The dimeric adiponectin bands were visualized by Western blotting with goat antiadiponectin antibody (R&D Systems) and quantified by densitometric intensity, which increased linearly from 1.0 to 25 μg/L. We detected a strong positive correlation (n = 19, r = 0.940) between the total adiponectin values determined by the 2 methods.

In all 19 samples, the LMW adiponectin was the dominant form of the 3 multimers (Table 1). In 16 of the 19 samples, the MMW or HMW concentrations were below the detection limits. In 3 samples, all 3 adiponectin multimers were detected. For these 3 samples, the mean (SD) ratios of HMW, MMW, and LMW (including Alb-LMW) to total adiponectin were significantly different from the reported values for the serum samples (n = 47): 0.18 (0.04) vs 0.39 (0.13), P <0.05; 0.15 (0.01) vs 0.27 (0.05), P <0.005; 0.69 (0.05) vs 0.34 (0.10), P <0.005, respectively, according to the Mann–Whitney U-test *(10)*.

To confirm these results, we separated the same CSF samples using 2%–15% native PAGE followed by Western blotting against adiponectin using goat antiadiponectin antibody *(10)*. The adiponectin multimers in the CSF samples were at the same positions as those of the serum adiponectin multimers (Fig. 1B). As expected, the CSF samples showed considerably weaker MMW and HMW bands and clearer Alb-LMW (double-stained) bands than those observed in the serum control *(7)*. Such double staining might result from hydroxylation or glycosylation of the Alb-LMW form *(13)*. Because the LMW form cannot be detected clearly in native PAGE analysis, we used nonheating SDS-PAGE analysis to separate the LMW form from CSF *(6)* and thus confirmed the existence of the LMW form in human CSF (Fig. 1C).

Finally, we examined whether protease A Amano and proteinase K selectively digest the CSF adiponectin multimers. We used native PAGE and Western blotting to analyze the digested products of CSF *(10)*. Consequently, we obtained HMW and MMW adiponectin after protease A Amano digestion and HMW adiponectin after proteinase K digestion (Fig. 1D). As with serum samples, these selective digestions enabled us to measure the 3 multimers in CSF samples.

The predominance of the smaller molecular forms in human CSF is supported by a recent report *(14)*. In men, but not in women, the CSF adiponectin concentrations correlated positively with serum adiponectin and negatively with body mass index. Furthermore, adiponectin receptors were detected in the brain *(4, 5)*. These results suggest that the presence of CSF adiponectin did not result from contamination with peripheral blood during CSF sampling.

In conclusion, our modified ELISA system is sufficiently sensitive for measuring CSF adiponectin, and it can measure the 3 multimers. Although LMW (including Alb-LMW) adiponectin was found to be the dominant form in this set of human CSF samples, HMW and MMW adiponectin multimers were also detected in some samples. Additional studies are required to clarify how the adiponectin multimers are transported across the blood–brain barrier and whether they play central roles in energy homeostasis. Our modified ELISA system will serve as a useful tool for future studies using CSF samples.

Table 1. Adiponectin concentrations in human CSF.[a]

Sample no.	Age	Sex	Adiponectin concentration, μg/L			
			Total	HMW	MMW[b]	LMW[c]
1	67	F	19.4	1.1	<1.0	17.3
2	32	F	4.6	<1.0	<1.0	4.6
3	66	F	6.8	1.0	<1.0	5.7
4	53	F	19.1	4.2	3.1	11.8
5	74	M	5.2	<1.0	<1.0	5.2
6	52	M	2.7	<1.0	<1.0	2.7
7	60	F	1.0	<1.0	<1.0	1.0
8	15	F	24.7	3.9	3.4	17.5
9	69	M	6.4	<1.0	<1.0	6.4
10	53	F	16.1	2.6	2.2	11.3
11	52	M	3.5	1.0	<1.0	2.5
12	23	M	1.3	<1.0	<1.0	1.3
13	39	F	5.9	1.3	<1.0	4.1
14	64	M	2.6	<1.0	<1.0	2.6
15	37	M	1.0	<1.0	<1.0	1.0
16	41	F	1.6	<1.0	<1.0	1.6
17	70	F	7.9	<1.0	1.4	5.9
18	42	M	5.9	<1.0	<1.0	5.9
19	72	M	1.7	<1.0	<1.0	1.7

[a] CSF was obtained from 19 subjects with normal CSF cell counts and laboratory tests. The total and 3 multimer adiponectin concentrations were determined using the ELISA described in the text. HMW, high molecular weight form; MMW, middle molecular weight form; LMW, low molecular weight form.
[b] MMW = (MMW + HMW) − HMW.
[c] LMW = total − (MMW + HMW).

Grant/funding support: None declared.
Financial disclosures: None declared.

References

1. Scherer PE, Williams S, Fogliano M, Baldini G, Lodish HF. A novel serum protein similar to C1q, produced exclusively in adipocytes. J Biol Chem 1995;270:26746–9.
2. Yamauchi T, Kamon J, Waki H, Terauchi Y, Kubota N, Hara K, et al. The fat-derived hormone adiponectin reverses insulin resistance associated with both lipoatrophy and obesity. Nat Med 2001;7:941–6.
3. Matsuda M, Shimomura I, Sata M, Arita Y, Nishida M, Maeda N, et al. Role of adiponectin in preventing vascular stenosis: the missing link of adipo-vascular axis. J Biol Chem 2002;277:37487–91.
4. Qi Y, Takahashi N, Hileman SM, Patel HR, Berg AH, Pajvani UB, et al. Adiponectin acts in the brain to decrease body weight. Nat Med 2004;10:524–9.
5. Spranger J, Verma S, Gohring I, Bobbert T, Seifert J, Sindler AL, et al. Adiponectin does not cross the blood–brain barrier but modifies cytokine expression of brain endothelial cells. Diabetes 2006;55:141–7.
6. Waki H, Yamauchi T, Kamon J, Ito Y, Uchida S, Kita S, et al. Impaired multimerization of human adiponectin mutants associated with diabetes: